

# Bio-Inspired Strategies for Anti-Icing

Jianyong Lv, Yanlin Song, Lei Jiang, and Jianjun Wang\*

Institute of Chemistry, Chinese Academy of Sciences, Beijing 100190, P. R. China

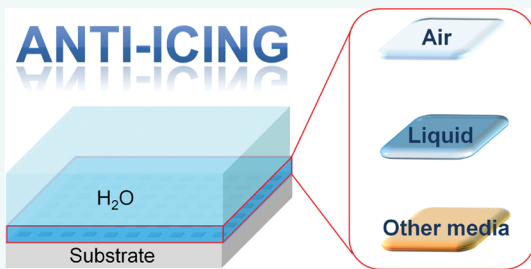
**ABSTRACT** Undesired ice accumulation leads to severe economic issues and, in some cases, loss of lives. Although research on anti-icing has been carried out for decades, environmentally harmless, economical, and efficient strategies for anti-icing remain to be developed. Recent researches have provided new insights into the icing phenomenon and shed light on some promising bio-inspired anti-icing strategies. The present review critically categorizes and discusses recent developments. Effectively trapping air in surface textures of superhydrophobic surfaces weakens the interaction of the surfaces with liquid water, which enables timely removal of impacting and condensed water droplets before freezing occurs. When ice already forms, ice adhesion can be significantly reduced if liquid is trapped in surface textures as a lubricating layer. As such, ice could be shed off by an action of wind or its gravity. In addition, bio-inspired anti-icing strategies *via* trapping or introducing other media, such as phase change materials and antifreeze proteins, are discussed.

**KEYWORDS:** bio-inspired · anti-icing · deicing · superhydrophobic · wettability · rebound · condensed microdroplet · coalescence induced self-removal · ice adhesion · lubricating layer

Icing and frosting cause inconvenience for the daily life of human beings.<sup>1</sup> Snowing and icing on roads result in slippery surfaces and often lead to traffic accidents. Andrey and Olley reported that about 40% of road accidents in winter were related to wetness, ice, or snow.<sup>2,3</sup> Icing on the wings and surfaces of aircrafts may cause crash accidents.<sup>4,5</sup> Aircrafts intercept supercooled water droplets when flying through clouds or encountering freezing rain and the impacting water freezes rapidly to form an ice accretion. The ice accretion results in drag increase and sometimes may lead to dangerous loss of lift force,<sup>6</sup> which may cause tragic crash accidents. For example, Flight 3407 recently crashed in Buffalo, NY, due to the rapid buildup of ice, which killed all 49 people on board and one person on the ground.<sup>7</sup> Transmission lines and power network towers may deform or even collapse with the burden of excess amount of ice. In 2008, a serious snow storm hit South China. In this disaster, 884 substations, 15 300 transmission lines, 184 000 high-voltage towers, and 519 000 low-voltage poles were broken,<sup>8,9</sup> and the direct economic loss was over 150 billion RMB.<sup>10</sup> Ice accretion on wind turbine blades can cause a production loss as much as 50% of the annual production.<sup>11</sup> The accreted ice increases the

load on the blades and the tower structure, leading to high amplitude vibration, turbine fatigue, mass imbalance, or even structural damages of the turbines.<sup>12,13</sup> Furthermore, frost and ice accumulation in refrigerators and heat exchangers results in a decrease of heat transfer efficiency.<sup>14</sup> It was reported that the decrease in heat transfer could be up to 50–75% due to the frost formation.<sup>15,16</sup> Therefore, great efforts have been made to understand the mechanism of icing and investigations on anti-icing and deicing have been extensively carried out.<sup>17–19</sup> Various anti-icing and deicing methods have been developed.<sup>17–22</sup> Unfortunately, conventional methods are often inefficient, costly, or environmentally harmful.

In this review, after briefly summarizing and discussing conventional anti-icing and deicing methods, we categorize recent progresses in bio-inspired anti-icing into three aspects as shown in Figure 1. Before freezing, in particular when supercooling is low (e.g.,  $-5^{\circ}\text{C}$ ), it takes some minutes or even hours for the supercooled water to be frozen. Thus, it would be possible to remove the impacting or condensed water droplets from solid surfaces before freezing occurs. We focus on the method of trapping air in surface textures of solid substrates to have superhydrophobic surfaces inspired



\* Address correspondence to  
wangj220@iccas.ac.cn.

Received for review December 20, 2013  
and accepted March 4, 2014.

Published online March 04, 2014  
10.1021/nn406522n

© 2014 American Chemical Society

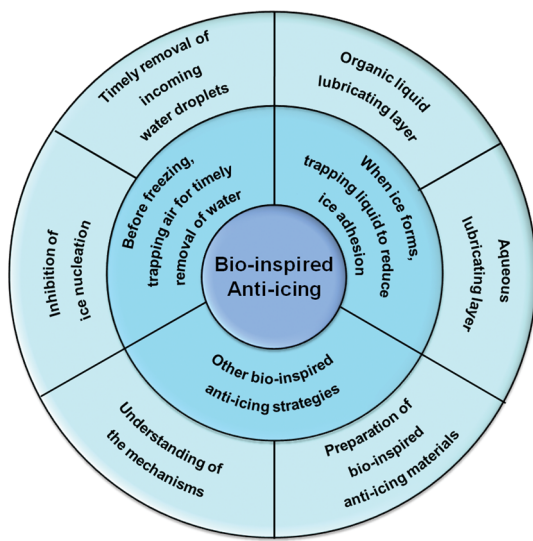


Figure 1. Three main categories of recently developed bio-inspired anti-icing strategies.

by lotus leaves and water strider legs, promoting timely removal of incoming water before freezing occurs. When ice is already formed, preventive preparation of surfaces with low ice adhesion for easy deicing is desirable. Inspired by the slippery peristome surface of *Nepenthes* pitcher plants, we discuss the strategy of trapping liquid as a lubricating layer between solid surfaces and accreted ice to reduce the interaction. Furthermore, it should be noted that living systems in subzero environments have developed powerful capability in anti-icing. We look into their anti-icing mechanisms, and discuss possible strategies of trapping or introducing other media to prepare new anti-icing materials. In each section, we highlight the recent significant developments and suggest future research directions.

**Conventional Methods for Anti-Icing and Deicing.** Keeping the surface temperature thermally above the freezing point in icing conditions is an effective anti-icing method. Electrothermal method exhibits to be an efficient strategy to prevent ice formation or accelerate ice melting. Especially for the anti-icing and deicing of transmission lines, utilization of the Joule effect for heating line conductors is recognized worldwide to be the most efficient engineering approach.<sup>18</sup> However, high cost for the equipment and energy consumption has to be taken into consideration. In addition, this method relies on the passage of electric flow, which results in new problems like electromagnetic disturbance to the operation of the apparatus.

Chemical method is the most popular strategy in anti-icing and deicing. An effective way is using freezing point depressants, which are often commercially available. Organic liquids whose crystallization temperatures are much lower than that of water are widely applied on the surface of aircrafts to prevent icing and frosting.<sup>21</sup> However, short duration of this approach

**VOCABULARY:** **anti-icing** – properties of materials or strategies for preventing or delaying freezing of the impacting and condensed water as well as decreasing the ice adhesion; **deicing** – removal of accreted ice, snow, or frost from a surface; **superhydrophobicity** – the property of surfaces being water-repellent including high water contact angle ( $>150^\circ$ ), low contact angle hysteresis, and ability to rebound incoming droplets; **heterogeneous ice nucleation** – formation of ice nucleus at preferential sites when liquid water phase contacts and/or contains other phases and/or other foreign species; **coalescence induced self-removal** – spontaneous self-removal of coalesced condensed microdroplets *via* converting released surface energy to kinetic energy; **liquid lubricating layer** – a film containing a certain amount of liquid which is able to lubricate two solid surfaces by reducing/preventing the interfacial wear, friction, and interaction;

leads to an inefficient periodic treatment of extended surfaces and extensive usage of such liquids may cause various environmental problems. Salts are often used to melt ice and snow on the roads in winter. Due to the high solubility of NaCl, it is reported that 75–90% of the added salt enters the roadside environment *via* runoff or splashing.<sup>23</sup> Ground water can be contaminated by the infiltration of the salt solution.<sup>24,25</sup> In addition, roadside vegetations, as well as water creatures living alongside the roads, are seriously affected.<sup>26</sup> Recently a sol–gel technology was developed to be able to reduce the application frequency<sup>27,28</sup> and ease the damage to environments. However, this technology is limited for practical applications due to the high cost.

Mechanical deicing method is often applied to remove ice from apparatuses that are easily approached, such as overhead transmission lines and power networks, by either directly scraping to break ice accretion or utilizing the energy released by shock waves, vibrations, or twisting of conductors.<sup>18</sup> This method often requires that people get direct access to the lines and towers. When the ice is less accessible, helicopters or even shotguns are makeshifts.<sup>17</sup> During deicing, mechanical force causes extra stress to the networks and leads to failure in some cases. Therefore, mechanical deicing is neither safe nor efficient.

Low surface energy polymer coatings, like poly(tetrafluoroethylene),<sup>29,30</sup> poly(dimethylsiloxane),<sup>31</sup> and polymer composites with nanoparticles,<sup>32</sup> are often applied to prepare hydrophobic or superhydrophobic surfaces, which cannot be wetted by water. In some cases, water accumulation on these coating surfaces could be prevented and the interaction of the surfaces with ice is weakened. Varanasi *et al.* tested the ice adhesion strength of a series of low surface energy polymer coatings and polymer/POSS composite coatings.<sup>33</sup> Most of these coatings exhibited reduced ice adhesion strength of 200–500 kPa as compared to 698 kPa of the bare steel surface.<sup>33</sup> To date, a wide

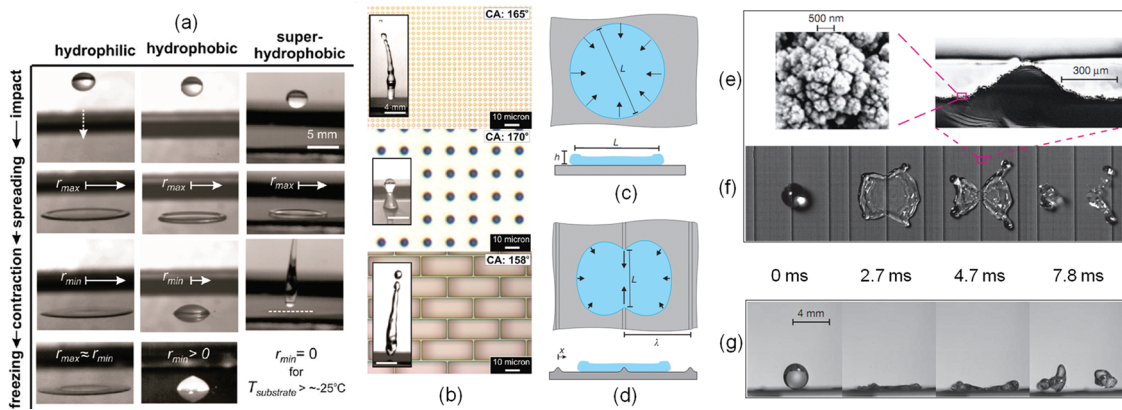


**Figure 2.** (a) Sequential images of the dynamic behavior of  $15\ \mu\text{L}$  water droplets impacting cooled ( $<0\ ^\circ\text{C}$ ) horizontal surfaces from a 10 cm height. Pinning and freezing were observed on hydrophilic and smooth hydrophobic surfaces, while full retraction and rebound of the droplet was observed on the SHS. (b) Optical images of (top, middle) open-cell nanopost structures and (bottom) a closed-cell brick structure taken normal to the surface. Insets show dynamic retraction behavior of  $\sim 15\ \mu\text{L}$  droplets impacting from a 10 cm height at room temperature. Surfaces with (top) small spacing posts and (bottom) bricks remain superhydrophobic and repel the droplets, while the surface with (middle) larger spacing posts shows low pressure stability and fails upon droplet impacting, leading to wetting. CA indicates the approximate value of the advancing contact angle formed by a droplet on the substrate. Panels a and b are adapted with permission from ref 49. Copyright 2010 American Chemical Society. (c) Top-view and side-view diagrams illustrating the retraction behavior of impacting droplet on the SHS without the macrostructure. (d) Top-view and side-view diagrams illustrating the retraction behavior of impacting droplet on the SHS with a macrostructure of ridges. (e) SEM images of the surface morphology of the silicon SHS with a macrostructure. (f) High-speed images captured from the top-view of the spread and retraction behavior of impacting droplet on SHS with a macrostructure. (g) High-speed images captured from the side-view of the spread and retraction behavior of impacting droplet on SHS with a macrostructure. Panels c–g are reprinted by permission from ref 58. Copyright 2013 Macmillan Publishers Ltd.: *Nature*; <http://www.nature.com/nature>.

range of coatings claiming anti-icing are commercially available. Ice adhesion strengths of almost all the commercial coatings were tested to be broadly ranged in 230–1400 kPa as compared to 1576 kPa of the bare aluminum surface.<sup>34</sup> The only one exception was a two-component silicon elastomer dispersed in xylene, which resulted in a coating with ice adhesion strength of 40 kPa,<sup>34</sup> whereas Cohen *et al.* pointed out that this coating should be a sacrificial coating containing unreacted oligomers that could be shed off with the formed ice.<sup>35</sup>

In addition, many other anti-icing and deicing methods have been studied and applied. Automatic robots,<sup>18</sup> electromagnetic forces,<sup>13</sup> electro-impulse,<sup>20</sup> and high voltage direct current<sup>22</sup> are reported for the deicing of overhead lines. Flexible pneumatic boots are often installed on aircrafts to break accreted ice layers.<sup>21,36</sup> Investigations in using microwave for deicing have been carried out, but this method has not yet been successfully implemented.<sup>17,36</sup> Thus, most of these conventional anti-icing and deicing strategies are often inefficient, energy-consuming, high-cost, or environmentally harmful. To conquer these problems, the development of environmentally harmless, economical, and efficient strategies for anti-icing and deicing is an urgent need.

**Trapping Air for Timely Removal of Water.** Superhydrophobic surfaces (SHSs) mimicking lotus leaves<sup>37,38</sup> and water strider legs<sup>39</sup> usually have nanostructure and/or microstructure with air trapped inside the surface textures.<sup>40–42</sup> On SHSs, deposited water droplet stays at a nonwetting Cassie–Baxter state<sup>43</sup> and has large

contact angle ( $>150^\circ$ ), small contact angle hysteresis,<sup>44</sup> and small contact area with the solid surface.<sup>40,44</sup> Ascribed to the trapped air, interaction between water droplet and the solid surfaces is minimized, and the water droplet slides easily on an SHS when the surface is slightly tilted.<sup>45,46</sup> In addition, the energy barrier of removing water droplets from an SHS is decreased. Quéré *et al.* for the first time demonstrated that SHSs were of practical interest for anti-icing because deposited water droplets could be gravitationally removed from subzero SHSs before freezing when there was a tilting angle.<sup>47</sup> Icing usually originates from the freezing of impacting water droplets and condensed water droplets, and removal of these two types of water before freezing will be discussed below.

**Rebound of Impacting Water Droplets.** The unique characteristics of SHSs result in complete retraction and elastic rebound of impacting water droplets.<sup>48</sup> Thus, it is possible to utilize SHSs in subzero environments to rebound impacting water droplets to prevent water accumulation before freezing. As demonstrated in Figure 2a, the impacting droplets attached and froze on hydrophilic and hydrophobic surfaces due to the incomplete retraction.<sup>49</sup> Interestingly, the droplet completely retracted and timely rebounded off before freezing on the SHS.<sup>49</sup> This phenomenon raises two fundamental questions for exploring the timely rebound of impacting water droplets on SHSs for anti-icing applications.

The first question is the following: could an impacting droplet rebound on all SHSs, and if it rebounds,

how long does it take for the droplet to retract and rebound? When a water droplet impacts on an SHS, energy can be stored in the spreading stage due to the small residual hysteresis.<sup>50</sup> The stored energy can be scaled as  $\sigma R^2 \Delta \cos \theta$  ( $\sigma$  is the liquid–gas surface tension,  $R$  is the droplet radius,  $\theta$  is the mean contact angle of water drop on the SHS, and  $\Delta \cos \theta$  is contact angle hysteresis).<sup>50</sup> Quéré *et al.* concluded that if the droplet kinetic energy which scales as  $\rho R^3 V^2$  ( $\rho$  is liquid density,  $V$  is impacting velocity) is larger than the stored energy, the droplet rebounds.<sup>50</sup> This implies that only “large enough” droplets or/and droplets with high enough velocity can rebound. For example, it was found that for  $V = 1$  m/s, the critical radius of rebound droplets is of the order of  $100 \mu\text{m}$ .<sup>50</sup>

Complete retraction and rebound of impacting droplets require that the trapped air in surface textures is stable and the SHS is not wetted under impacting to keep the surface superhydrophobic. The wetting state of a textured surface is dependent on the balance of wetting pressure ( $P_{\text{wetting}}$ ) and antiwetting pressure ( $P_{\text{antiwetting}}$ ).<sup>51,52</sup> If  $P_{\text{wetting}}$  is larger than  $P_{\text{antiwetting}}$ , impacting of water droplets on SHSs can lead to a transition from Cassie–Baxter state to partial Wenzel or complete Wenzel state,<sup>53</sup> and the water wets the surface textures.<sup>52</sup> On one hand,  $P_{\text{wetting}}$  is determined by the impacting velocity of droplets.<sup>52</sup> For a certain solid surface, enhanced impacting velocity results in an increase of  $P_{\text{wetting}}$ , which may destroy the composite solid–air–liquid interface by pushing out the trapped air from surface textures.<sup>54</sup> The critical value of impacting velocity is dependent on the geometric parameters of the surface.<sup>54</sup> Above this critical velocity, droplets partially or even fully wet the surface textures after impacting and will not be able to completely rebound, especially for nanopatterned SHSs because of the small amount of trapped air as compared to SHSs with micro textures.<sup>54</sup> On the other hand,  $P_{\text{antiwetting}}$  is the capillary pressure generated within surface textures and is related to the surface morphology.<sup>52</sup> As shown in Figure 2b, at the same impacting velocity, surfaces with dilute structures tended to be partially or fully wetted and the droplet could not rebound due to the relatively low  $P_{\text{antiwetting}}$ .<sup>49,52</sup>

However, SHSs with well designed surface structures can prevent the wetting of surface textures by the impacting water droplets. Most recently, Poulikakos *et al.* systematically investigated water droplets impacting on subzero micro-, nano-, and hierarchical structured SHSs.<sup>55</sup> And the impacting behaviors were characterized by Weber number ( $We$ ) defined as eq 1:<sup>55</sup>

$$We = \frac{\rho V^2 D_0}{\sigma} \quad (1)$$

where  $\rho$  is the liquid density,  $\sigma$  is its surface tension,  $V$  is the droplet impacting velocity, and  $D_0$  is the droplet diameter. It was found that there was a critical value of

Weber number,  $We_c$ , beyond which impacting droplets could not completely rebound.<sup>55</sup> Importantly,  $We_c$  was much higher for SHSs with hierarchical structures as compared to micro- or nanostructured SHSs.<sup>55</sup> A hierarchical SHS with minimal surface texture spacing could resist droplet penetration at  $We$  of 227 (corresponding to an impacting velocity of 2.6 m/s).<sup>55</sup> We should note that the surface structures mentioned above are all open-cell structures. And the stability of SHSs can be further improved on closed-cell structured SHSs. Aizenberg *et al.* evaluated the rebound behavior of impacting water droplets on SHSs with a open-cell nanopost structure and a closed-cell brick structure as shown in Figure 2b.<sup>49</sup> Air was trapped in the closed-cell brick structure and could not be pushed out even at an extremely high impacting velocity of 90–135 m/s.<sup>49</sup> Additionally, the closed-cell structured SHS is more mechanically robust and has the potential to be employed due to the easy preparation *via* soft lithography and imprinting.<sup>49</sup>

Quéré *et al.* studied the rebound behavior of water droplets vertically impacting on an SHS by varying the impacting velocity and droplet radius.<sup>56,57</sup> As described by eq 2, it was found that contact time ( $t_c$ ) is independent of the impacting velocity in a wide range (20–230 cm/s) and is related to the initial drop radius ( $R_0$ ) and liquid–gas surface tension ( $\sigma$ ).<sup>56</sup> According to eq 2, if an impacting droplet can completely rebound from a certain solid surface,  $t_c$  is a constant when the droplet size is fixed. For a  $15 \mu\text{L}$  droplet impacting on a superhydrophobic silicon substrate, Aizenberg *et al.* observed a critical transition temperature, above which impacting droplets could rebound, to be  $-20 \sim -25^\circ\text{C}$ .<sup>49</sup> Below this transition temperature, the droplet froze within a time less than  $t_c$ .

$$t_c = 2.65 \left( \frac{\rho R_0^3}{\sigma} \right)^{1/2} \quad (2)$$

Most recently, Varanasi *et al.* proposed that  $t_c$  could be further reduced if the SHSs were well designed.<sup>58</sup> In the researches of Quéré *et al.*, impacting droplet spread to a nearly uniform film and retracted almost axisymmetrically as shown in Figure 2c. If macrostructures, such as ridges, with an amplitude comparable to (but less than) the film thickness were added to the SHS, retraction of impacting droplet could be separated into several parts as shown in Figure 2d. As demonstrated in Figure 2d–g, the droplet impacting on the macrostructured SHS resulted in a thinner film.<sup>58</sup> The retraction fronts moved faster along the peak of the macrostructure and the water film opened along the ridge, resulting in a fragmented water film.<sup>58</sup> Therefore, the distance for the separated water film to retract was decreased, leading to a shorter retraction time, which reduced  $t_c$  as compared to that on an SHS without macrostructures.<sup>58</sup>

We must emphasize here that in evaluating the rebound of impacting droplets on an SHS, variation of wettability with temperature and relative humidity was often neglected in literatures. As a matter of fact, the wettability of water on solid surfaces can be changed with decreasing the temperature and increasing the relative humidity. In a microscopic view, water molecules can be adsorbed on solid surfaces despite of the hydrophobicity. Wu *et al.* observed a nanoscale hydrophobic–hydrophilic transition on the inner walls of single wall nanotubes (SWNTs) with decreasing the temperature from 22.1 to 8.0 °C.<sup>59</sup> At the temperature lower than 8.0 °C, the adsorbed water molecules form an ordered monolayer structure on the inner walls of SWNTs. The water binding energy, *i.e.*, the potential-energy difference of the system in a given configuration with and without the water molecules, is narrowly distributed inside the nanotube. The states of the low binding energy, which dominate the free energy, are less frequently occupied, resulting in a lower chemical potential than that of the saturated vapor.<sup>59,60</sup> Thus, substantial adsorption could happen even below the saturated vapor pressure at 8.0 °C.<sup>59</sup> When the temperature is lowered, the arrangement of adsorbed surface water may change, which could lead to the change of the surface wettability.<sup>61,62</sup>

In a macroscopic view, water condensation occurs on solid surfaces when the temperature decreases to the dew-point. During the condensation, water drop grows as  $\langle R \rangle \sim t^{1/D_d}$  (isolated drops) and  $\langle R \rangle \sim t^{1/(D_d-D_s)}$  (coalescing drops), where  $R$  is the drop radius,  $t$  is time, and  $D_d$  and  $D_s$  are the dimensionality of the water drops and the substrate structure, respectively.<sup>63,64</sup> On surfaces with microscale structures, condensed water droplets nucleate both on the top of and between the textures despite of the hydrophobicity, and even more water could be accumulated between the textures.<sup>64</sup> In this situation, condensation leads to Wenzel water drops even on SHSs<sup>65</sup> and the surfaces become hydrophilic. Once SHSs lose their superhydrophobicity, impacting droplets cannot rebound. Here the loss of superhydrophobicity presents a challenge: how to keep the superhydrophobicity of a surface even when condensation occurs. Wang *et al.* found that if the surface area fraction of the solid surface is equal to or smaller than 0.068, an SHS can remain superhydrophobic at the dew-point.<sup>66</sup>

The second question is how long does it take for a droplet in contact with a cold solid surface to be frozen? Freezing of a water droplet is a two-stage process including nucleation and growth of the critical nucleus. The formation and afterward the growth of the formed critical nucleus may take some time, *i.e.*, so-called induction time of crystallization;<sup>67</sup> therefore, water can be supercooled to a temperature lower than the equilibrium temperature. The instant homogeneous nucleation generally occurs at the temperature

approximately below –40 °C.<sup>68</sup> In practice, factors affecting freezing are multiple and complicated, and the homogeneous nucleation is difficult to achieve because of the presence of foreign materials like impurities and substrates. At low supercooling, freezing on solid surfaces occurs first *via* heterogeneous ice nucleation at the interface, and the nucleation is usually the control process.<sup>47,69,70</sup> If the heterogeneous ice nucleation could be inhibited, water droplets stay longer at the liquid state. However, some impurities can act as nuclei to initiate rapid icing of water.<sup>71</sup> Additionally, evaporative cooling at the liquid–gas interface could affect the freezing when there is an unsaturated gas flow. In this case, the temperature at the liquid–gas interface is dramatically decreased and rapid partial solidification is observed.<sup>71</sup>

For the investigation of the effects of solid surfaces on the nucleation, it should be noted that possible impurities in water and on substrate may remarkably hinder clarifying the exact effects of the substrate on the ice nucleation. Wang and co-workers designed an evaporation–condensation setup to observe the nucleation of thousands of condensed water microdroplets.<sup>72</sup> In a sealed clean sample cell, a water macrodroplet was placed at the edge of a thoroughly cleaned substrate. The water was first evaporated to create a saturated atmosphere. With decreasing temperature, microdroplets condensed onto the substrate surface. Then ice nucleation events of large amounts of separate and independent condensed water microdroplets could be studied using a high speed camera. In this evaporation–condensation process, influence of possible impurities was greatly minimized.<sup>72</sup> Therefore, it provides reliable information on kinetic and thermodynamic details of ice nucleation and it is possible to further the understanding on the nucleation mechanism.

**Self-removal of Condensed Water Droplets.** Accumulation of impacting water droplets on SHSs can be avoided due to the rebound resulting from the initial kinetic energy. However, in humid environments, removal of condensed microdroplets is still a challenge. Chilled solid surfaces can accumulate water through the rapid condensation. On SHSs, condensed droplets with the size comparable to the capillary length may be removed under gravity *via* tilting the surfaces. But the condensed microdroplets usually stay and freeze eventually on the surfaces because gravity does not work at this regime. To remove the condensed microdroplets before freezing, new strategies have to be developed.

Ballistospore discharge is an interesting feature for many species of basidiomycete yeasts. As shown in Figure 3a,<sup>73</sup> the Buller's drop develops at the base of the spore, and a film of liquid accumulates on the side of the spore (Figure 3a, top). When the drop and the liquid film increase to a critical size and coalesce, the coalesced drop and the spore jump away (Figure 3a,

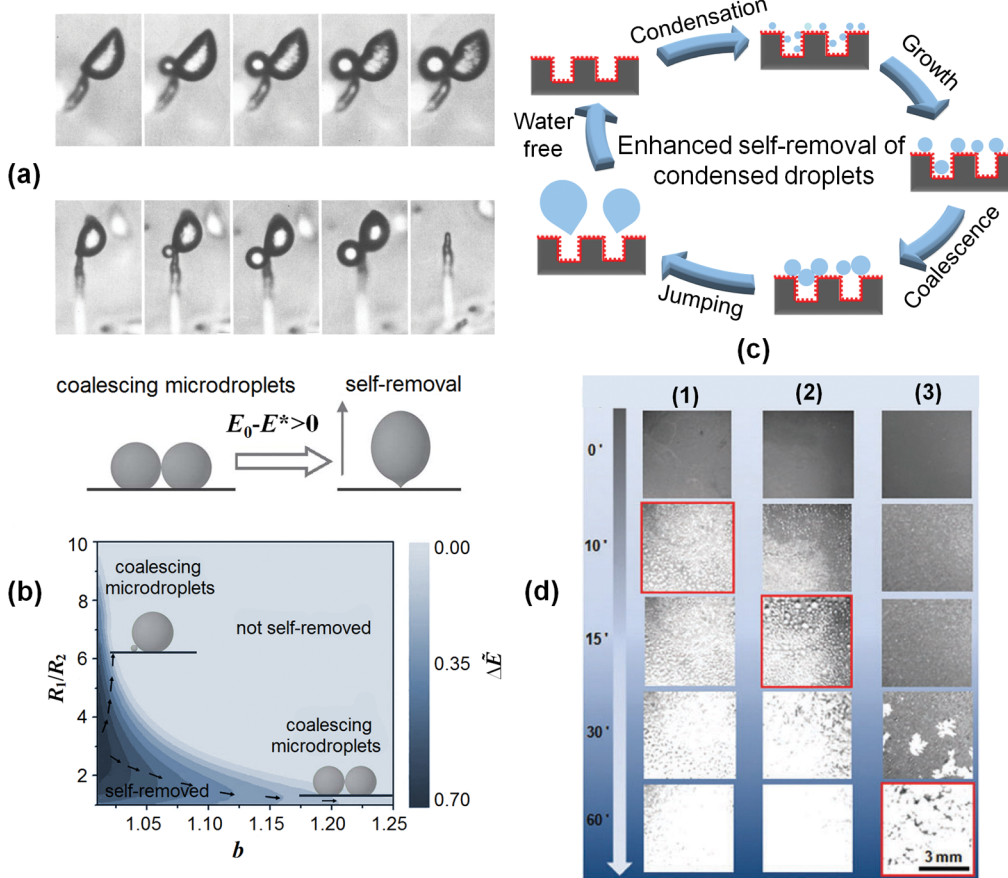


**Figure 3.** (a) Mechanism of ballistospore discharge. (Top) The Buller's drop develops at the base of the spore and a film of liquid accumulates on the side of the spore, which can be confirmed by the change in outline of the spore. (Bottom) Successive images illustrate the growth of Buller's drop at the base and the liquid film on the side surface of the spore. In the final frame, simultaneous disappearance of the drop and the spore from sterigma is observed after the drop and liquid film increase to a critical size and coalesce. Reprinted with permission from ref 73. Copyright 1984 Elsevier. (b) (Top) Schematic illustration of the coalescence induced self-removal.  $E_0$  is the initial total surface energy and  $E^*$  is the critical energy barrier. (Bottom) The necessary condition for microdroplets to be self-removed after coalescence. As the prefactor  $b$  increases, the  $R_1/R_2$  approaches unity. If  $b$  is larger than  $b_c = 2^{1/3} = 1.26$ , the self-removal could not occur anymore. Adapted with permission from ref 76. Copyright 2012 The Royal Society of Chemistry. <http://pubs.rsc.org/en/content/articlelanding/2012/sm/c2sm25828e#!divAbstract> (c) Schematic illustration of condensation on the nanostructured superhydrophobic surface with a micropore array at a high supersaturation. (d) The process of ice/frost formation on (1) a normal aluminum surface, (2) a nanostructured SHS, and (3) an SHS with a  $10 \mu\text{m}$  micropore array through a digital camera. The images highlighted by red lines indicate that the entire surface is covered by the frost layer. The high supersaturation was  $6.97$  ( $T_{\text{surface}} = -15^\circ\text{C}$ ). The environmental temperature was  $25 \pm 0.8^\circ\text{C}$  and the relative humidity was  $42.3 \pm 2.6\%$ . (c and d) Adapted with permission from ref 82. Copyright 2013 The Royal Society of Chemistry. <http://pubs.rsc.org/en/content/articlelanding/2013/cc/c3cc40592c#!divAbstract>.

bottom) driven by the released surface energy.<sup>74</sup> This coalescence induced spontaneously jumping away behavior of liquid drops can be termed as coalescence induced self-removal. Chen *et al.* observed an out-of-plane self-removal of coalesced water microdroplets on appropriately designed SHSs and the jumping velocity of the droplets could be as high as  $1 \text{ m/s}$ .<sup>75</sup>

Inspired by this phenomenon, anti-icing materials were prepared by fabricating surfaces from which condensed water droplets can spontaneously jump away before freezing. Wang *et al.* concluded that adhesion of condensed water microdroplets to solid substrates is the dominant energy barrier during the coalescence induced self-removal<sup>76</sup> judging from the Ohnesorge number ( $Oh$ ), which is the ratio between

viscous force and interfacial tension force as shown in eq 3:<sup>77</sup>

$$Oh = \frac{\mu}{\sqrt{\rho\sigma D}} \quad (3)$$

where  $\mu$  is the shear viscosity of the fluid,  $\sigma$  is the liquid–gas surface tension,  $\rho$  is the liquid density, and  $D$  is the droplet diameter. When  $Oh < 0.1$ , the viscosity effect is negligible,<sup>77</sup> which indeed is the case for the self-removed condensed microdroplets.<sup>78</sup> If the coalescence released surface energy overcomes the work of adhesion ( $W_{\text{ad}}$ , integration of the contact line pinning force over the unit area), which is the main energy barrier, coalescence induced self-removal of droplets occurs. Wang and co-workers prepared a series of solid

surfaces with different  $W_{ad}$ , and studied the coalescence induced self-removal behaviors of the condensed microdroplets.<sup>76</sup> It was observed that the self-removal efficiency of condensed droplets decreases with the increase of  $W_{ad}$ . The coalescence induced self-removal could be theoretically analyzed by the model presented in Figure 3b, where  $E_0$  represents for the initial total surface energy ( $E$ ) of two microdroplets, and  $E^*$  is an introduced critical energy barrier. When  $E_0 > E^*$ , the coalesced microdroplets could be removed from the solid surface. This could be further transferred to the following equation eq 4:<sup>76</sup>

$$\Delta\tilde{E} = \frac{E_0 - E^*}{a_0 R_2^2} = 1 + x^2 - b(1+x^3)^{2/3} \geq 0 \quad (4)$$

where  $a_0$  is a positive constant which is dependent on the chemical composition and physical morphology of the solid surface but is independent of the radius of microdroplets,  $x$  is the radius ratio of the two coalescing microdroplets ( $R_1:R_2$ ) and we can set  $R_1 \geq R_2$  without any loss in generality,  $b$  ( $b > 1$ ) represents the shape deviation of the microdroplet from a perfect sphere and increases with  $W_{ad}$ . As presented in Figure 3b, coalescence induced self-removal will not occur any more when  $b$  is larger than 1.26, which agrees very well with the experimental observation.<sup>76</sup>

Patrick Collier *et al.* reported that condensed water microdroplets on SHSs were able to be self-removed before heterogeneous ice nucleation could occur.<sup>79</sup> And the coalescence induced self-removal of the condensed microdroplets could not occur until the diameter of the droplets reaches about 10  $\mu\text{m}$ .<sup>79</sup> At higher supersaturation or lower temperature, water condenses both on the top of and at the bottom of surfaces textures and wet the surface.<sup>80</sup> Condensed microdroplets tend to stay in the high adhesion Wenzel state rather than Cassie–Baxter state,<sup>81</sup> and self-removal efficiency is reduced. By utilizing the pinning effects of three phase contact line, Wang *et al.* successfully enhanced the self-removal efficiency of condensed water microdroplets under high supersaturation. A series of micropore arrays were introduced on nanostructured SHSs.<sup>82</sup> The pore size varied from 6 to 14  $\mu\text{m}$ , and periodicity of the pores was 20  $\mu\text{m}$ . Both the pore size and periodicity were at the same order of magnitude with that of the condensed water microdroplets, so that the air fraction beneath water droplets was maximized and interaction of the condensed water microdroplets with solid substrate was minimized. As demonstrated in Figure 3c, growing condensed water microdroplets are pinned at the edges of the micropores.<sup>82</sup> Thus, the shapes of these condensed microdroplets deviate from spheres and the coalesced microdroplets accumulate more surface energy; at the same time, because of the three phase contact line pinning, there is less contact area between the microdroplets and the substrates, which leads to a less

energy barrier to be overcome for coalescence induced self-removal. Experimental results showed that introduction of micropore arrays indeed facilitated the coalescence induced self-removal of condensed microdroplets. The surface with 10  $\mu\text{m}$  pore array showed the highest jumping frequency and the diameter of removed microdroplets was smallest on this surface.<sup>82</sup> It was observed that droplets even with a diameter smaller than 5  $\mu\text{m}$  could be self-removed. That is smaller than the size of the coalescing microdroplets in jumping events on the nanostructured SHS at low supersaturation and much smaller than the size of the condensed microdroplets sliding away from a lubricating film (hundreds of micrometers).<sup>82</sup>

Due to the timely drainage of condensed water *via* coalescence induced self-removal, frost does not form on ideal SHSs at all.<sup>79</sup> Unfortunately, frost can be initiated at the defects on the SHSs.<sup>79</sup> As soon as frost is formed, it grows by generating an ice bridge to the neighboring drops *via* interdrop frost waves to induce a chain reaction of frosting which proceeds to cover the whole surfaces.<sup>79,83,84</sup> However, frost growth can be delayed *via* the self-removal of condensed water droplets by limiting the formation of interdrop ice bridges.<sup>79,85</sup> As presented in Figure 3d, due to the effective self-removal of condensed microdroplets, Wang *et al.* observed that it took about 1 h for the entire hierarchical micropore arrayed-SHS to be covered by frost as compared to 8 and 14 min of the normal aluminum surface and the nanostructured aluminum SHS, respectively, and during this period, the amount of formed frost was decreased by 1.2  $\text{kg}/\text{m}^2$ .<sup>82</sup>

**Trapping Liquid To Reduce Ice Adhesion.** As presented above, at low supercooling, trapping air in the surface textures of solid substrate can achieve the timely removal of impacting and condensed water droplets before freezing. When ice is already formed, an alternative is to fabricate low ice adhesion surfaces on which formed ice can be easily shed off under an action of gravity, wind force, or vibration. Trapping liquid as a lubricant between the substrate surface and formed ice enables substantial weakening of the interaction between the ice and the solid surface, which can reduce the ice adhesion significantly and render it able to shed off the ice by an action of wind or its own gravity.

**Mechanism and Characterization of Ice Adhesion.** SHSs were regarded for some years as the most attractive strategy for preparing anti-icing materials.<sup>32,41,42,86–88</sup> Reports showed that ice adhesion strength on SHSs was significantly lowered.<sup>89,90</sup> The mainly accepted explanation for the low ice adhesion strength on SHSs is that water freezes in Cassie–Baxter state and forms a “Cassie ice or frost”.<sup>35,91</sup> For example, it was reported that SHS with nanostructures could promote the formation of frost in the suspended Cassie state.<sup>91</sup> In this case, air trapped beneath the droplets is

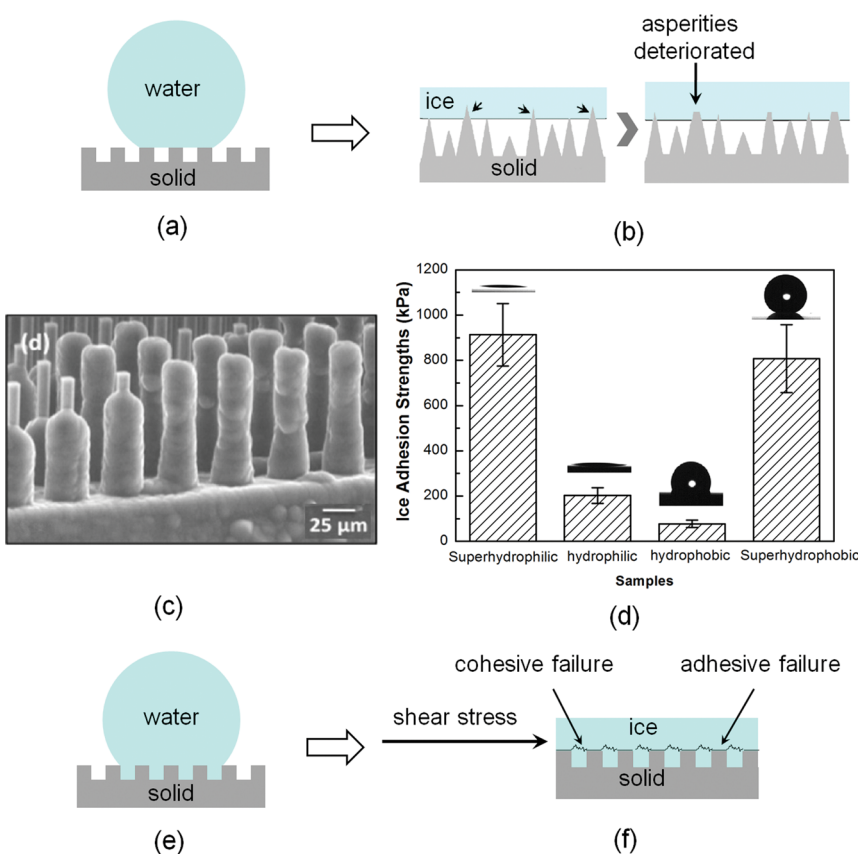


**Figure 4.** (a) Cassie–Baxter state of water droplets on a solid surface. (b) (Left) Ice on a superhydrophobic anti-icing surface. The textures with tips penetrated into the ice (indicated by arrows) are very likely to be damaged during icing (water solidification) and/or deicing (ice removal). (Right) Ice on the same surface sitting lower on the textures during the next icing events. The ice–solid contact area increases from (left) to (right). Adapted with permission from ref 92. Copyright 2011 American Chemical Society. (c) ESEM images of frost formation on a superhydrophobic surface comprising of an array of hydrophobic square posts. The intrinsic water contact angle of the hydrophobic coating on the posts is  $\sim 110^\circ$ . The surface temperature is  $-13^\circ\text{C}$ . Adapted with permission from ref 94. Copyright 2010, AIP Publishing LLC. (d) Average ice adhesion strengths on four silicon wafer surfaces with different hydrophobicities measured at  $-15^\circ\text{C}$ . Insets are the profiles of water droplets on the corresponding surfaces. Adapted with permission from ref 96. Copyright 2012, AIP Publishing LLC. (e) Wenzel state of water droplets on a solid surface. (f) Schematic illustration of the ice adhesion strength for removing the ice from a patterned substrate. Adapted with permission from ref 96. Copyright 2012, AIP Publishing LLC.

maintained after freezing and the real contact area between the “Cassie ice or frost” and solid surface is reduced. Therefore, the contact area dependent adhesive interaction between ice and substrate is minimized. However, even if “Cassie ice or frost” can be formed, SHSs are of notable limitation for the practical application. As shown in Figure 4a, water droplets at Cassie–Baxter state sit atop of the surface textures of SHSs.<sup>92</sup> The surface textures usually do not have the same height. When water freezes, ice layer and surface textures partially interpenetrate. Thus, the surface textures could be destroyed during the deicing process as shown in Figure 4b<sup>92</sup> and the superhydrophobicity deteriorates after several icing/deicing cycles.<sup>92,93</sup>

Actually, SHSs do not necessarily result in “Cassie ice or frost” at freezing conditions, especially for microstructured SHSs. An extreme case is the frosting of water vapor. As demonstrated in Figure 4c, Varanasi *et al.* observed that, under a high supersaturation condition, frosting rapidly occurred and frost directly

accrued between microscale surface textures of the SHS,<sup>94,95</sup> which led to an enhancement in surface wettability. Therefore, condensed and impacting water droplets easily accumulated and the formed ice layer penetrated into the textures, which increased ice adhesion greatly. Wang *et al.* systematically investigated the influences of surface morphology and chemical composition on the ice adhesion strength. As shown in Figure 4d,<sup>96</sup> it was observed that ice adhesion strengths on structured surfaces are much higher than that on flat surfaces regardless of the chemical composition.<sup>96</sup> SHSs may lose their superhydrophobicity as aforementioned when water adsorption and condensation occur. Condensation could lead to Wenzel water drops as shown in Figure 4e. In this case, a strongly interlocking “Wenzel ice”<sup>35</sup> can be formed after freezing as demonstrated in Figure 4f. Once “Wenzel ice” is formed, the real contact area between ice and the rough surface is significantly increased and the ice layer interlocks with surface textures. When investigating the ice adhesion

strength parallel to the solid surface, removal of the ice layer from the surface needs to overcome the adhesive strength between the ice and substrate as well as the cohesive strength of ice itself. This mechanism can be described by eq 5:<sup>96</sup>

$$\tau = \tau_{coh} \times \phi + \tau_{adh} \times (1 - \phi) \quad (5)$$

where  $\tau$  is the apparent ice adhesion strength on rough surfaces,  $\tau_{coh}$  is the cohesive strength of ice (about 1600 kPa<sup>97</sup>),  $\tau_{adh}$  is the adhesive strength of ice on an ideal flat surface, and  $\phi$  is the area fraction of the ice layer interlocking with the surface textures. Because the cohesive strength of the ice is much larger than the adhesive strength, the mechanical interlocking dominates the apparent ice adhesion.

It seems to be a paradox because some research groups claimed that SHSs showed a reduced ice adhesion while others stated that SHSs presented an increased ice adhesion. To clarify the relationship between superhydrophobicity and "icephobicity" of a surface, Nosonovsky *et al.* started from the concepts of these two terms and carried out a comparative study of parameters related to superhydrophobic and "icephobic" surfaces. It is summarized that superhydrophobicity and "icephobicity" of a surface are parallel rather than directly correlated.<sup>98</sup> In other words, superhydrophobic does not always mean "icephobic".<sup>98,99</sup>

Here we would like to point out the absence of a standardized procedure for the characterization of ice adhesion strength could also be a reason that ice adhesion strengths on SHSs differ in literatures. On one hand, preparation methods of ice samples are different. Spraying supercooled water droplets to substrates in a wind tunnel can effectively mimic the icing or frosting process in the natural environment. However, it is not applicable for most of laboratories due to the high cost of the setup. Pouring supercooled water onto substrates is simple but of poor reproducibility. Parameters like temperature, velocity, and amount of the droplets have considerable effects on the wetting state and the real ice-substrate contact area. In addition, the quality of water used to prepare ice samples also has to be taken into consideration because of possible impurities. On the other hand, the methods used to evaluate the ice adhesion strength are different in the literatures. A few groups characterized the ice adhesion strength by measuring the normal force *via* vertically pulling the ice samples off the substrates.<sup>88,100,101</sup> In this case, the measured values contained only the contribution of the normal adhesive strength rather than the shear strength between ice and the substrate. Some groups froze ice on a rotating horizontal beam of a centrifuge apparatus.<sup>102–104</sup> The centrifugal force of detaching ice was used as the ice adhesion strength. Some researchers measured the shear strength of propelling ice off from the substrate.<sup>33,105</sup> The shear strength for detaching the ice

layer formed between an inner cylindrical pin and an outer cylindrical mould was also used to evaluate the ice adhesion strength.<sup>106</sup> The consequence is that the testing results based on different evaluation criteria are not comparable. We suggest that the definition of ice adhesion strength needs to be unified. For instance, the ice adhesion strength calculated by eq 6 can be an acceptable option:

$$\text{Adhesion strength} = F/A \quad (6)$$

where  $F$  is the shear force for detaching the ice from a solid surface, and  $A$  is the apparent contact area (cross-sectional area) between the ice and the substrate. In addition, the preparation method of ice samples, the testing procedure, and the evaluation criterion of the ice adhesion strength should be standardized.

**Trapping Organic Liquid Lubricating Layer.** Aizenberg *et al.* developed a slippery liquid-infused porous surface (SLIPS)<sup>107</sup> inspired by *Nepenthes* pitcher plants.<sup>108</sup> A water-immiscible lubricating organic liquid was trapped in the surface textures to have a molecularly smooth surface with low water contact angle hysteresis.<sup>107</sup> This methodology is applicable to various inexpensive and low-surface-energy structured materials like Teflon and epoxy resin. Fabrication process of SLIPS is illustrated in Figure 5a.<sup>107</sup> On a substrate coated by porous polymers, a certain amount of perfluorinated fluid was infused to form a continuous liquid lubricating layer. When water droplet deposited on SLIPS, a composite solid–lubricant–water interface forms and the droplet slides easily at a small tilting angle. Even in a high humidity environment (e.g., 60% relative humidity), SLIPS coated substrates remain ice/frost repellent by effectively removing the condensed water. When the deposited water freezes, as shown in Figure 5b left,<sup>109</sup> the trapped organic liquid acts as an intermediary lubricating layer to prevent the penetration of frost/ice into the surface textures and lead to an extremely low ice adhesion strength of only  $15.6 \pm 3.6$  kPa.<sup>110</sup> It was also tested statistically that the freezing of supercooled water on SLIPS coating could be depressed and the coating performance was not affected at all even after 150 freeze–thaw cycles.<sup>111</sup> Additionally, by selecting proper lubricants, the prepared SLIPS could be omniphobic to prevent the contaminants such as oil and blood. Furthermore, SLIPS is inherently smooth, optically transparent, wear-resistant, self-healing, and pressure resistant.<sup>112</sup> To date, no synthetic surfaces possess all these unique characteristics of SLIPS, and it is believed that SLIPS is of great potential to be applied in anti-icing, antifouling, optical devices, and other areas that are beyond the reach of current technologies.<sup>107,112</sup>

Varanasi *et al.* found that external forces such as gravity could drain the excess liquid to attain a thermodynamically stable configuration of the surface.<sup>113,114</sup> The ice adhesion strength on this equilibrated SLIPS

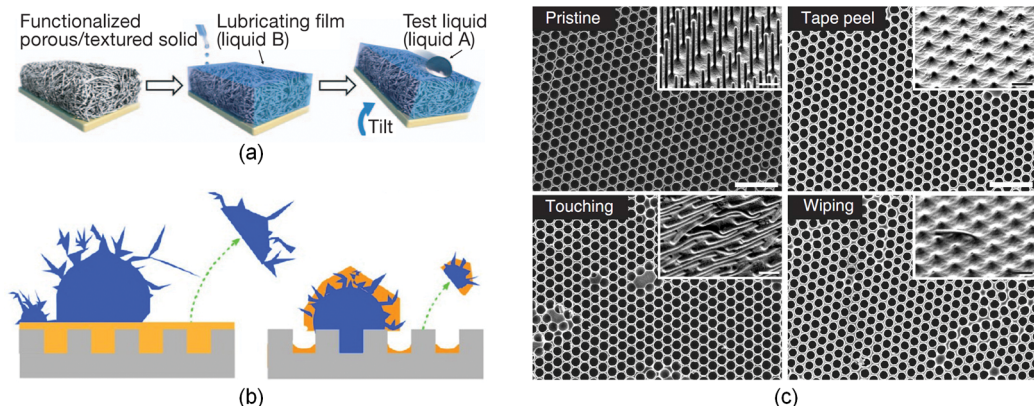


**Figure 5.** (a) Schematics showing the fabrication of SLIPS by infiltrating a functionalized porous/textured solid with a low-surface-energy, chemically inert liquid to form a physically smooth and chemically homogeneous lubricating layer on the surface of the substrate. Reprinted by permission from ref 107. Copyright 2011 Macmillan Publishers Ltd.: *Nature*. <http://www.nature.com/nature>. (b) Different schematics of frosting and defrosting on SLIPS described by (left) Aizenberg *et al.* and (right) Varanasi *et al.* Adapted with permission from ref 109. Copyright 2013 American Chemical Society. (c) Mechanical stability of the closed-cell, inverse monolayers shown by SEM images of surface structures after subjection to different mechanical treatments. The inverse monolayer coating withstands touching, wiping, and tape peel tests, while open-cell reference samples (epoxy micropillars; shown for comparison as insets) are completely damaged by all treatments. All scale bars are 5  $\mu$ m. Reprinted by permission from ref 116. Copyright 2013 Macmillan Publishers Ltd.: *Nature Communications*. <http://www.nature.com/ncomms>.

was dramatically higher than that on SLIPS with excess liquid, although the value of the ice adhesion strength was still lower as compared to a smooth surface coated with 80/20 PEMA-FluoroPOSS<sup>33</sup> which was considered to be one of the lowest surface energy materials.<sup>114</sup> In addition, frost or ice formed on SLIPS was not always afloat on the liquid film.<sup>109,115</sup> Driven by capillary attraction, lubricant migrated from the wetting ridge and the substrate's texture to the frozen droplet's surface (Figure 5b right).<sup>109</sup> In this case, lubricant could be gradually depleted during deicing or defrosting cycles as shown in Figure 5b right, and SLIPS failed in lubricating.<sup>109</sup>

Recently, Aizenberg *et al.* reported that the thermodynamical stability of SLIPS could be improved by employing a closed-cell architecture.<sup>116</sup> The lubricants could be firmly locked in the structures and the lubricant-infused layers demonstrated excellent thermodynamical stability of over 9 months vertical storage. It was tested that ice adhesion strength on this surface was only  $10 \pm 7$  kPa.<sup>116</sup> In addition, because of the rigid nature of the layer, the closed-cell SLIPS was mechanically stable as shown in Figure 5c.<sup>116</sup> The SLIPS with closed-cell structures could tolerate various mechanical treatments such as touching, wiping, and tape peeling. This was in strong contrast to the open-cell SLIPS which was completely destroyed after these mechanical treatments.<sup>116</sup>

**Trapping Aqueous Lubricating Layer.** It is also desirable to have a coating on which the lubricating layer forms naturally once icing occurs and remains as long as ice stays atop. Here it is worth to mention that the slippery rim of *Nepenthes* pitcher plants is caused by the condensed water or rainwater on the hygroscopic nectar at the peristome surface.<sup>108</sup> Therefore, water is

an alternative to be used as a lubricating liquid. Furthermore, it is known that ice has slippery surfaces, and because of this, ice sports, such as skating, are possible. At the ice surface, the hexagonal structure of ice breaks down and a liquidlike layer is formed even at temperatures below 0 °C (Figure 6a).<sup>117,118</sup> Due to the existence of the lubricating liquid water layer,<sup>119</sup> the adhesion strength of ice to skate blades is significantly reduced and people can skate with grace. This mechanism is of great potential to be used for anti-icing.

We propose that the following requirements need to be met before the aqueous lubricating layer can be utilized as coatings: (1) The aqueous layer should be able to work in a large temperature range below 0 °C. (2) Appropriate thickness of the aqueous layer is necessary so that the surface asperities could be covered by the aqueous layer and the mechanical interlocking could be completely prevented. (3) The coatings should be mechanically robust or/and self-healing.

On the basis of above requirements, a robust prototypical organic–inorganic composite anti-icing coating with an aqueous lubricating layer is designed as illustrated in Figure 6b.<sup>105</sup> Cross-linked hygroscopic polymer, poly(acrylic acid) (PAA) as a demonstration, is incorporated into the micropores of a porous silicon wafer, because the hygroscopic polymers lower the freezing and melting points. Sorption of water by the hygroscopic polymers from the moisture or the melted ice formed atop leads to a water-swollen polymer layer which bulges out of micropores. The swollen polymers merge together due to the molecular attraction and form a continuous aqueous lubricating layer. When icing occurs, direct contact between ice and solid surface is prevented by the continuous aqueous lubricating layer, and the ice adhesion strength is

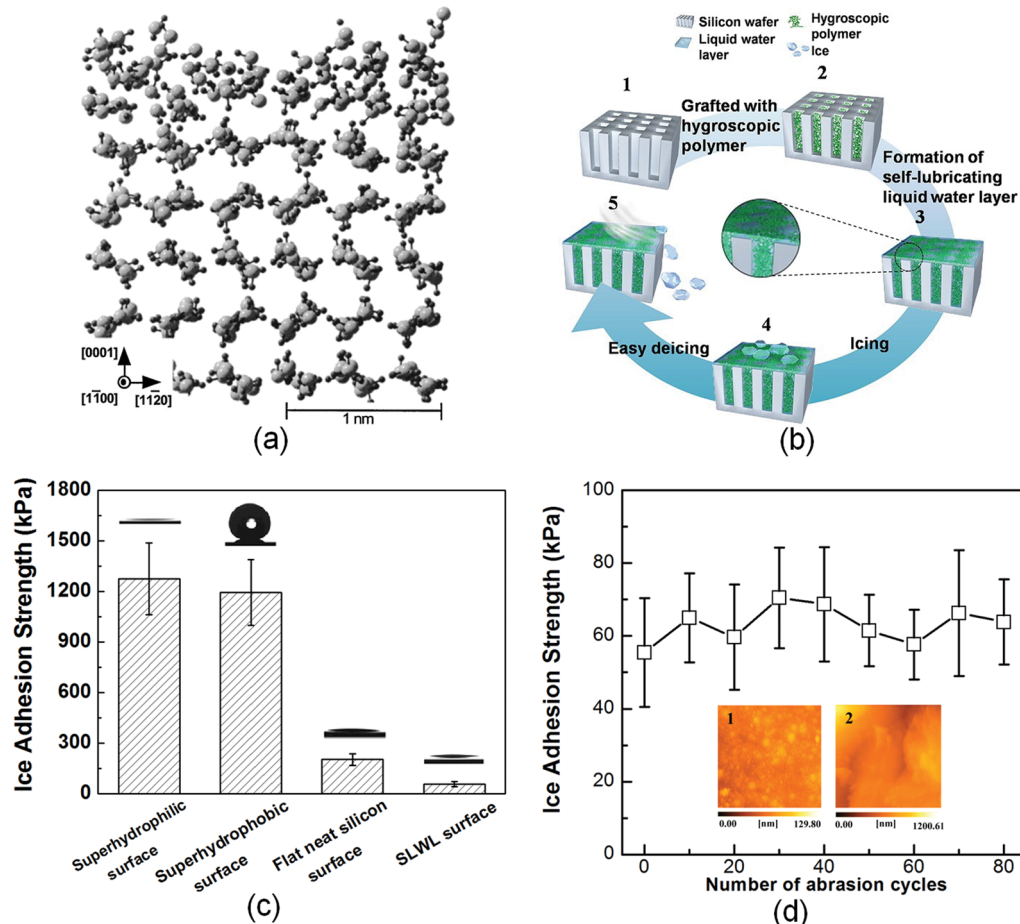


**Figure 6.** (a) Melting layer on ice surface observed by molecular-dynamics calculation. The large gray and the small black circles show the oxygen and hydrogen atoms, respectively. The thin lines are the covalent bonds. Reprinted with permission from ref 117. Copyright 2004 AIP Publishing LLC. (b) Schematic illustration of the preparation of the self-lubricating liquid water layer surface. (1) Fabrication of micropore arrayed silicon wafer surfaces *via* a photolithographic process. (2) Grafting the micropore arrayed silicon wafer surfaces with cross-linked hygroscopic polymers. (3) Self-lubricating liquid water layer forms on micropore arrayed silicon wafer surfaces when condensation or deliquesce occurs. Inset is the magnified image of self-lubricating liquid water layer. (4) Ice formation atop of the self-lubricating liquid water layer. (5) Ice shed off with a wind action. (c) Average ice adhesion strengths on four surfaces with different hydrophobicity. Insets are the profiles of water droplets on the corresponding surfaces. (d) Average ice adhesion strengths on the anti-icing surface with self-lubricating liquid water layer remained almost the same after several tens cycles of abrasion test with a normal loading of 12.5 kPa by a 10 000 mesh sandpaper, which clearly shows that the fabricated anti-icing surface have the capability of self-healing and abrasion resistance. The insets are Atomic force microscopy images ( $2 \mu\text{m} \times 2 \mu\text{m}$ ) of the area between pores on the SLWL surface (1) before and (2) after abrasion. (b–d) Adapted with permission from ref 105. Copyright 2013 American Chemical Society.

remarkably lowered as compared to those on superhydrophobic and superhydrophilic silicon surfaces with the same porous morphology as shown in Figure 6c.<sup>105</sup>

Here it is worth to mention that the hygroscopic polymer depresses the freezing temperature and the melting temperature of water because it lowers the water activity.<sup>120</sup> Although there is a phase transition temperature ( $-28^\circ\text{C}$ ) shown in that paper, below which ice adhesion strength increased sharply due to the freezing of the aqueous layer, this transition temperature can be further reduced by selecting the polymer type and varying the concentration of the polymer network in the micropores.<sup>105</sup> Thus, the composite coating can be designed to be adaptable for

extremely low temperature environments. In addition, this organic–inorganic composite coating is of significant potential for long-term application. On one hand, water in aqueous layer could be continuously resupplied to the hygroscopic polymers by the moisture or ice melting. On the other hand, the organic–inorganic prototype coating is mechanically robust. Ice adhesion strength remains almost the same even after 80 cycles of abrasion with sandpapers (Figure 6d).<sup>105</sup>

**Trapping or Introducing Other Media for Anti-Icing.** Living systems in subzero environments, including polar fish,<sup>121</sup> insects,<sup>122,123</sup> bacteria,<sup>124,125</sup> and plants,<sup>126,127</sup> fight against icing with their unique ways. Afro-alpine plant *Lobelia telekii*, which lives in high alpine zones of Mount Kenya, has about 1 L viscous liquid inside the

hollow inflorescence. This liquid contains highly potent ice nucleators and may freeze at the temperature just below 0 °C.<sup>128</sup> Then the heat released from freezing can be used as a protective heat source. Although other Afro-alpine plants of the genera *Lobelia* and *Senecio* do not have any water inside the inflorescences, they can trap rainwater between the rosette leaves to achieve heat protection in a similar way with *L. telekii*.<sup>129</sup> In addition, some temperate region plants can tolerate freezing in winter with potent ice nucleating agents in their extracellular fluid. On the basis of the similar mechanism, heat storage materials utilizing latent heat have been developed. Salt hydrates and alkane/aliphatic solutions based phase change materials (PCMs) are trapped in polymer or stainless steel balls and sealed,<sup>130</sup> and the released latent heat can be utilized when phase change of these materials occurs. Although the cost may be high at present, we can visualize the application of phase change materials *via* utilizing the released latent heat for anti-icing.

Additionally, dimensional change accompanying the phase change of PCMs could also be employed for anti-icing. An anti-icing coating was reported by formulating silicone PCM particles within hydrophobic resins.<sup>131</sup> Cooled by the cold air, a solid–solid phase change occurs over a narrow temperature range. The PCMs expand and at the same time the substrate contracts. When water freezes, released latent heat is absorbed by the PCMs and results in another inverse solid–solid phase change. Then the ice-coating interface experiences a large local shear stress due to the volume change of the coating layer. It is claimed that the actual lateral local displacements of the surface could reach  $1/10$  the diameter of the PCM particles, which is enough to locally break the ice–surface bond.<sup>131</sup> Thus, the ice could be detached, and afterward the coating cooled by the cold air again, and the cycle repeats. Although no information of commercial coatings utilizing PCMs for anti-icing is available, the concept proposed is enlightening.

Many fishes and insects living in subzero environments have antifreeze proteins (AFPs) or antifreeze glycoproteins (AFGPs) in their blood plasma. With the help of these proteins which can inhibit the ice growth,<sup>132,133</sup> the fishes and insects can survive through the harsh winter. The well-accepted mechanism of inhibiting the ice growth is the adsorption–inhibition mechanism.<sup>134,135</sup> First, the AFPs are able to recognize and bind “quasi-irreversibly” to the ice surface. Then the growth of ice is confined in between the absorbed proteins with a curved interface.<sup>136</sup> The interfacial curvature results in a reduction of local freezing temperature due to the Kelvin effect, while leaving the melting temperature unaffected.<sup>136,137</sup> Usually, the thermal hysteresis (TH) temperature, difference between the freezing and melting temperature, is used to describe the antifreeze activity of an

AFP or AFGP. TH of AFPs and AFGPs extracted from the blood of polar fish is usually 2 °C, whereas insect AFPs can exhibit TH of over 5 °C.<sup>137,138</sup>

Recently, Francis *et al.* incorporated a Type III AFP (T3AFP) from ocean pout fish and a snow flea AFP (SnAFP) into polymer chains through site-selective coupling to prepare an anti-icing coating.<sup>139</sup> The homogeneity of resulting materials was improved and individual proteins were able to function in a uniform manner.<sup>139</sup> Schematic illustration of the preparation of polymer–AFP coating is demonstrated in Figure 7a.<sup>139</sup> Ice formation and growth on the glass coated by polymer–AFP were significantly inhibited and delayed. As shown in Figure 7b, it took only 20 min for condensed water to be frozen on surfaces without polymer–AFP. As a contrast, complete freeze of condensed water was observed after 75 min on polymer–AFP coated surfaces. This strategy is of great potential to be further developed and employed for anti-icing/anti-frosting. Synthetic materials mimicking these proteins and their analogues are also in process in order to have the easy availability.<sup>140,141</sup>

In summary, media that are of potential to be introduced for anti-icing should be of the following characteristics: (1) If a medium can reduce the interaction of substrate surfaces with incoming water or even separate the surfaces from incoming water, it would be possible to prevent water accumulation on the surfaces before freezing occurs. (2) If a medium can inhibit

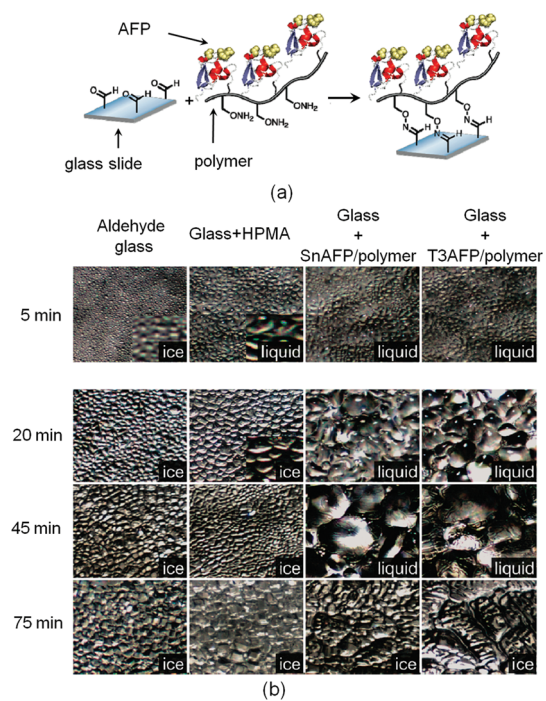


**Figure 7.** (a) Scheme of the polymer–AFP coating for anti-icing. (b) Coated glass slides were cooled to 6.0 °C at controlled humidity. Condensed water froze significantly faster on samples without the proteins. Images were collected at 40× magnification. Adapted with permission from ref 139. Copyright 2010 American Chemical Society.

the heterogeneous ice nucleation or delay the ice growth, it would be effective to avoid or retard icing on the substrate surfaces. (3) If a medium can decrease or eliminate the interaction of the surfaces with the formed ice, the ice layer would be easily removed from the surfaces at a extremely small load.

## CONCLUSIONS AND PERSPECTIVES

In this critical review, recently developed bio-inspired anti-icing strategies were highlighted and categorized into three types. Before freezing, anti-icing can be achieved by trapping air in surface textures of superhydrophobic surfaces to promote the rebound of impacting water droplets and coalescence induced self-removal of condensed water droplets. This strategy is valid in particular when the supercooling is low and it takes some time for the supercooled water to be frozen. When icing occurs, an effective anti-icing strategy is proposed *via* trapping liquids as lubricants between solid surface and formed ice to significantly reduce the ice adhesion. Thus, the formed ice can be easily shed off by an action of wind or gravity. In addition, trapping or introducing other media such as phase change materials and antifreeze proteins are of great potential for anti-icing in practical applications and fundamental research as well.

Superhydrophobic surfaces inspired by lotus leaves and water strider legs are utilized for the timely removal of incoming water before freezing. The superhydrophobicity is defined by high water contact angle ( $CA > 150^\circ$ ), low CA hysteresis, and the ability to rebound impacting water droplets.<sup>98</sup> Low CA hysteresis corresponds to low surface water interaction such as the contact line pinning, integration of which over unit area represents the work of adhesion of liquid water with the solid surfaces. Here we want to point out the fourth aspect, that is, the ability to have coalescence induced self-removal of condensed water microdroplets or even nanodroplets, which is crucial for broad applications such as enhancement of heat transfer, anti-icing and self-cleaning at supersaturated environments. The wettability of solid surfaces is determined by both the chemical composition and the geometrical structure of the surfaces.<sup>142</sup> Substantial water adsorption occurs at the supersaturated environments. And the local structure of adsorbed surface water varies with the temperature, which affects the wettability of condensed water microdroplets and nanodroplets. Thus, a correlation between surface water structure and the wettability needs to be established. It is known that at the nanoscale the energy barrier between the Cassie state and the Wenzel state is so small that the thermal fluctuation could cause a transition between these two states.<sup>143</sup> Thus, the geometrical requirement of hierarchical microstructure and nanostructure of superhydrophobicity for

macroscopic drops needs to be revised in the case of condensed microscopic and nanoscopic droplets.

How to suppress the ice formation during the time that incoming water (impacting and condensed water) stays in contact with solid surface is another interesting scientific problem. This can be transferred to the problem of how to inhibit heterogeneous ice nucleation initiated at liquid–solid interface, because heterogeneous ice nucleation is the control step in the process of ice formation in this situation.<sup>69</sup> It has been suggested that the heterogeneous nucleation of a liquid in contact with solid surface can be controlled by the lateral structure of the interface layer.<sup>144</sup> Schülli *et al.* experimentally observed that supercooling in gold–silicon (AuSi) eutectic droplets was enhanced by a Au-induced ( $6 \times 6$ ) reconstruction of the Si(111) substrate.<sup>145</sup> How to structure the interface water that can tune the nucleation of liquid water atop is intriguing not only for anti-icing applications but also for cryopreservation of cells and tissues, preventing the freezing of crops, cloud seeding, and snow making.

Inspired by the slippery peristome surface of *Nepenthes* pitcher plants, trapping aqueous lubricating layer is very promising for significantly reducing the ice adhesion, so that the formed ice could be shed off by an action of wind or its own gravity. Aqueous lubricating layer has long-term durability because the lubricant is water, which can be continuously resupplied by water adsorption, condensation, and ice melting. Importantly, utilizing water as the lubricant is eco-friendly and economical. The thickness and viscosity of the lubricating layer affect crucially on the ice adhesion strength.<sup>118</sup> Therefore, correlations between the ice adhesion and the thickness as well as the viscosity of the aqueous lubricating layer need to be established, which are currently undergoing in our group.

In addition to the strategies discussed above, smart interface materials would be interesting for anti-icing. For example, a recent paper reported that a carbon dioxide vapor film could be generated *via* sublimation upon the impact of water droplet on the dry ice surface, thus the direct contact of the surface with the droplet could be avoided.<sup>146</sup> Therefore, the interaction between the underneath solid surface and the water were could be greatly reduced, and the liquid water could be removed before freezing occurred. This is inspiring because it could be attempted to introduce certain substances, which generate gases when they meet liquid water or ice, onto the solid surfaces for anti-icing. Other example could be smart polymers.<sup>147</sup> Temperature sensitive polymer, such as poly(*N*-isopropyl acrylamide) (PNIPAAm), can change the volume and surface morphology at the temperature (25–40 °C) due to conformational change of the polymer chains and this change is reversible.<sup>147,148</sup> Although this temperature range in which conformational change occurs is far above the freezing point of water, it can be

foreseen that smart polymers sensitive to the freezing temperature will be eventually developed for anti-icing. For practical technical applications, it is often not enough to achieve desired anti-icing effect only utilizing one strategy. Multiple strategies need to be combined for effective anti-icing. As aforementioned, if water drops partially or completely stay at the sticky Wenzel state on SHSs, rebound of impacting droplets and self-removal of the condensed droplets are affected or even cannot occur before freezing. External forces can be used for dewetting the surfaces to retain their superhydrophobicity. It was reported that mechanical vibration can overcome the energy barrier and induce a transition from Wenzel state to Cassie state of water droplets on a lotus leaf.<sup>149</sup> In addition, external electric field could be potentially used to enhance the jumping performance of the droplets to prevent water accumulation because the jumping water droplets carry net positive charges.<sup>78</sup> When ice already formed, for example on the surface with an aqueous lubricating layer, ultrasound vibration could be applied to facilitate the ice removal as soon as only a very thin ice sheet is formed.

Due to the fragility of micro- or/and nanosurface structures, one of the key challenges for bio-inspired surfaces and interface materials is to improve the stability and mechanical robustness. Investigations on fabricating stable and mechanically robust SHSs have been vastly carried out in the recent years.<sup>150–157</sup> However, few reports focused on SHSs with designed closed-cell geometries (e.g., honeycomb structure) which could serve better stability and mechanical robustness.<sup>49</sup> Recently, it was reported that the SLIPS with rigid closed-cell architectures demonstrated excellent thermodynamical stability and damage tolerance to various mechanical treatments.<sup>116</sup> In addition to the structure design, preparing organic–inorganic composite surfaces can be another choice.<sup>105</sup> Another challenge is the facile and large-scale fabrication of bio-inspired surfaces and interface materials. For example, although a variety of methods for preparing SHSs have been developed,<sup>158,159</sup> few of those methods really meet the facile and large scale criteria. Varanasi *et al.* reported that some rare-earth oxides could be applied to prepare robust large-scale hydrophobic ceramic materials and could also be used to fabricate superhydrophobic surfaces.<sup>160</sup> However, additional factors were required to achieve the robustness of superhydrophobic surfaces.<sup>160</sup> As such, further efforts need to be taken to prepare low-cost, large-scale bio-inspired surfaces and interface materials with excellent properties.<sup>41,42,44,161</sup>

Although this review is oriented toward practical applications, there exist fundamental scientific challenges, for example, how to inhibit ice nucleation and growth on solid surfaces, what is the dominant mechanism for the ice adhesion, and how to achieve low

ice adhesion surfaces. All these are scientific challenges with a long history, and some of them have existed for more than 150 years. Anti-icing provides an excellent platform to systematically look into all these questions, and this review is expected to serve as a touchstone for further investigations in the future.

*Conflict of Interest:* The authors declare no competing financial interest.

*Acknowledgment.* J.W. acknowledges sincerely the beneficial discussion with Prof. Dr. G. Wegner at Max-Planck Institute for Polymer Research. The authors are grateful for the financial support from the Chinese National Nature Science Foundation (Grant Nos. 51173196, 21004068, 21121001) and the 973 Program (2012CB933801, 2013CB933004).

## REFERENCES AND NOTES

1. Björnstad, U.; Björnstad, J.; Dahlgren, A. Slipping on Ice and Snow—Elderly Women and Young Men Are Typical Victims. *Accid. Anal. Prev.* **1997**, *29*, 211–215.
2. Andrey, J.; Olley, R. The Relationship between Weather and Road Safety: Past and Future Research Directions. *Clim. Bull.* **1990**, *24*, 123–136.
3. Andersson, A. K.; Chapman, L. The Impact of Climate Change on Winter Road Maintenance and Traffic Accidents in West Midlands, UK. *Accid. Anal. Prev.* **2011**, *43*, 284–289.
4. Pike, W. S. Extreme Warm Frontal Icing on 25 February 1994 Causes An Aircraft Accident Near Uttoxeter. *Meteorol. Appl.* **1995**, *2*, 273–279.
5. Marwitz, J.; Politovich, M.; Bernstein, B.; Ralph, F.; Neiman, P.; Ashenden, R.; Bresch, J. Meteorological Conditions Associated with The ATR72 Aircraft Accident Near Rose-lawn, Indiana, on 31 October 1994. *Bull. Am. Meteorol. Soc.* **1997**, *78*, 41–52.
6. Gent, R. W.; Dart, N. P.; Cansdale, J. T. Aircraft Icing. *Philos. Trans. R. Soc. London, Ser. A* **2000**, *358*, 2873–2911.
7. Mosher, F. R.; Schaum, D.; Herbster, C.; Guinn, T. Analysis of Causes of Icing Conditions Which Contributed to the Crash of Continental Flight 3407. Presented at 14th Conference on Aviation, Range, and Aerospace Meteorology, Atlanta, GA, 17–21 January, **2010**.
8. Lu, J.; Jiang, Z.; Zhang, H.; Lei, H.; Li, B.; Fang, Z. Analysis of Hunan Power Grid Ice Disaster Accident in 2008. *Autom. Electr. Power Syst.* **2009**, *11*, 005.
9. Li, T.; Li, J. Analysis of Icing Accident in South China Power Grids in 2008 and Its Countermeasures. In *Electricity Distribution-Part 1, 2009. CIRED 2009. 20th International Conference and Exhibition on*, Prague, Czech Republic, 8–11 June, 2009; IET: London, **2009**.
10. Ministry of Civil Affairs of the People's Republic of China. Notification for General Information of Recent Freezing Rain and Snow Disasters and The Disaster Relief. <http://www.mca.gov.cn/article/special/xz/gzbs/200802/20080200011960.shtml>.
11. Botta, G.; Cavaliere, M.; Holttinen, H. Ice Accretion at Acqua Spruzza and its Effects on Wind Turbine Operation and Loss of Energy Production. In *Proceeding of the International Conference, Wind Energy Production in Cold Climate, BOREAS IV*, Hetta, Finland, March 31 – April 2, **1998**.
12. Frohboese, P.; Anders, A. Effects of Icing on Wind Turbine Fatigue Loads. *J. Phys.: Conf. Ser.* **2007**, *75*, 012061.
13. Dalili, N.; Edrisy, A.; Carriveau, R. A Review of Surface Engineering Issues Critical to Wind Turbine Performance. *Renewable Sustainable Energy Rev.* **2009**, *13*, 428–438.
14. Radermacher, R.; Kim, K. Domestic Refrigerators: Recent Developments. *Int. J. Refrig.* **1996**, *19*, 61–69.
15. Emery, A.; Siegel, B. Experimental Measurements of The Effects of Frost Formation on Heat Exchanger Performance. Presented at Proceedings of AIAA/ASME Thermo

Physics and Heat Transfer Conference, 18–20 June, Seattle, WA, **1990**.

- Huang, L.; Liu, Z.; Liu, Y.; Gou, Y.; Wang, J. Experimental Study on Frost Release on Fin-and-Tube Heat Exchangers by Use of a Novel Anti-Frosting Paint. *Exp. Therm. Fluid Sci.* **2009**, *33*, 1049–1054.
- Laforte, J. L.; Allaix, M. A.; Laflamme, J. State-of-The-Art on Power Line De-Icing. *Atmos. Res.* **1998**, *46*, 143–158.
- Farzaneh, M.; Volat, C.; Leblond, A. *Anti-Icing and De-Icing Techniques for Overhead Lines*; Springer: Netherlands, 2008; pp 229–268.
- Boinovich, L. B.; Emelyanenko, A. M. Anti-Icing Potential of Superhydrophobic Coatings. *Mendeleev Commun.* **2013**, *23*, 3–10.
- Egbert, R. I.; Schrag, R. L.; Bernhart, W. D.; Zumwalt, G. W.; Kendrew, T. J. An Investigation of Power Line De-Icing by Electro-Impulse Methods. *IEEE Trans. Power Delivery* **1989**, *4*, 1855–1861.
- Thomas, S. K.; Cassoni, R. P.; MacArthur, C. D. Aircraft Anti-Icing and De-Icing Techniques and Modeling. *J. Aircr.* **1996**, *33*, 841–854.
- Horwill, C.; Davidson, C.; Granger, M.; Dery, A. An Application of HVDC to the De-Icing of Transmission Lines. In *Transmission and Distribution Conference and Exhibition*, Dallas, TX, may 21–24, **2006**.
- Norrström, A. C.; Bergstedt, E. The Impact of Road De-Icing Salts (NaCl) on Colloid Dispersion and Base Cation Pools in Roadside Soils. *Water, Air, Soil Pollut.* **2001**, *127*, 281–299.
- Howard, K. W.; Haynes, J. Groundwater Contamination Due to Road De-Icing Chemicals–Salt Balance Implications. *Geosci. Can.* **1993**, *20*, 1–8.
- Williams, D. D.; Williams, N. E.; Cao, Y. Road Salt Contamination of Groundwater in A Major Metropolitan Area and Development of a Biological Index to Monitor Its Impact. *Water Res.* **2000**, *34*, 127–138.
- Sanzo, D.; Hecnar, S. J. Effects of Road De-Icing Salt (NaCl) on Larval Wood Frogs *Rana sylvatica*. *Environ. Pollut.* **2006**, *140*, 247–256.
- Ayres, J.; Simendinger, W. H.; Balik, C. M. Characterization of Titanium Alkoxide Sol-Gel Systems Designed for Anti-Icing Coatings: I. Chemistry. *J. Coat. Technol. Res.* **2007**, *4*, 463–471.
- Ayres, J.; Simendinger, W. H.; Balik, C. M. Characterization of Titanium Alkoxide Sol-Gel Systems Designed for Anti-Icing Coatings: II. Mass Loss Kinetics. *J. Coat. Technol. Res.* **2007**, *4*, 473–481.
- Menini, R.; Farzaneh, M. Elaboration of  $\text{Al}_2\text{O}_3/\text{PTFE}$  Icephobic Coatings for Protecting Aluminum Surfaces. *Surf. Coat. Technol.* **2009**, *203*, 1941–1946.
- Jafari, R.; Menini, R.; Farzaneh, M. Superhydrophobic and Icephobic Surfaces Prepared by RF-Sputtered Polytetrafluoroethylene Coatings. *Appl. Surf. Sci.* **2010**, *257*, 1540–1543.
- Zhu, L.; Xue, J.; Wang, Y.; Chen, Q.; Ding, J.; Wang, Q. Ice-Phobic Coatings Based on Silicon Oil Infused Polydimethylsiloxane. *ACS Appl. Mater. Interfaces* **2013**, *5*, 4053–4062.
- Cao, L.; Jones, A. K.; Sikka, V. K.; Wu, J.; Gao, D. Anti-Icing Superhydrophobic Coatings. *Langmuir* **2009**, *25*, 12444–12448.
- Meuler, A. J.; Smith, J. D.; Varanasi, K. K.; Mabry, J. M.; McKinley, G. H.; Cohen, R. E. Relationships between Water Wettability and Ice Adhesion. *ACS Appl. Mater. Interfaces* **2010**, *2*, 3100–3120.
- U.S. Army Corps of Engineers. *Ice Engineering*; University Press of the Pacific: Honolulu, HI, 2006; Chapter 20, pp 24–32.
- Meuler, A. J.; McKinley, G. H.; Cohen, R. E. Exploiting Topographical Texture To Impart Icephobicity. *ACS Nano* **2010**, *4*, 7048–7052.
- Parent, O.; Ilinca, A. Anti-Icing and De-Icing Techniques for Wind Turbines: Critical Review. *Cold Reg. Sci. Technol.* **2011**, *65*, 88–96.
- Jiang, L.; Zhao, Y.; Zhai, J. A Lotus-Leaf-like Superhydrophobic Surface: A Porous Microsphere/Nanofiber Composite Film Prepared by Electrohydrodynamics. *Angew. Chem.* **2004**, *116*, 4438–4441.
- D'Acunzi, M.; Mammen, L.; Singh, M.; Deng, X.; Roth, M.; Auernhammer, G. K.; Butt, H.-J.; Vollmer, D. Superhydrophobic Surfaces by Hybrid Raspberry-like Particles. *Faraday Discuss.* **2010**, *146*, 35–48.
- Gao, X.; Jiang, L. Biophysics: Water-Repellent Legs of Water Striders. *Nature* **2004**, *432*, 36–36.
- Sun, T.; Feng, L.; Gao, X.; Jiang, L. Bioinspired Surfaces with Special Wettability. *Acc. Chem. Res.* **2005**, *38*, 644–652.
- Yao, X.; Song, Y.; Jiang, L. Applications of Bio-Inspired Special Wettability Surfaces. *Adv. Mater.* **2011**, *23*, 719–734.
- Alizadeh, A.; Bahadur, V.; Kulkarni, A.; Yamada, M.; Ruud, J. A. Hydrophobic Surfaces for Control and Enhancement of Water Phase Transitions. *MRS Bull.* **2013**, *38*, 407–411.
- Cassie, A. B. D.; Baxter, S. Wettability of Porous Surfaces. *Trans. Faraday Soc.* **1944**, *40*, 546–551.
- Wong, T.-S.; Sun, T.; Feng, L.; Aizenberg, J. Interfacial Materials with Special Wettability. *MRS Bull.* **2013**, *38*, 366–371.
- Li, X. M.; Reinhoudt, D.; Crego-Calama, M. What Do We Need for A Superhydrophobic Surface? A Review on the Recent Progress in The Preparation of Superhydrophobic Surfaces. *Chem. Soc. Rev.* **2007**, *36*, 1350–1368.
- Deng, X.; Mammen, L.; Butt, H.-J.; Vollmer, D. Candle Soot as a Template for a Transparent Robust Superamphiphobic Coating. *Science* **2012**, *335*, 67–70.
- Tourkine, P.; Le Merrer, M.; Quéré, D. Delayed Freezing on Water Repellent Materials. *Langmuir* **2009**, *25*, 7214–7216.
- Richard, D.; Quéré, D. Bouncing Water Drops. *Europhys. Lett.* **2000**, *50*, 769–776.
- Mishchenko, L.; Hatton, B.; Bahadur, V.; Taylor, J. A.; Krupenkin, T.; Aizenberg, J. Design of Ice-Free Nanosstructured Surfaces Based on Repulsion of Impacting Water Droplets. *ACS Nano* **2010**, *4*, 7699–7707.
- Reyssat, M.; Pépin, A.; Marty, F.; Chen, Y.; Quéré, D. Bouncing Transitions on Microtextured Materials. *Europhys. Lett.* **2006**, *74*, 306–312.
- Bartolo, D.; Bouamrirene, F.; Verneuil, É.; Buguin, A.; Silberzan, P.; Moulinet, S. Bouncing or Sticky Droplets: Impalement Transitions on Superhydrophobic Micropatterned Surfaces. *Europhys. Lett.* **2006**, *74*, 299–305.
- Deng, T.; Varanasi, K. K.; Hsu, M.; Bhave, N.; Keimel, C.; Stein, J.; Blohm, M. Nonwetting of Impinging Droplets on Textured Surfaces. *Appl. Phys. Lett.* **2009**, *94*, 133109.
- Wenzel, R. N. Resistance of Solid Surfaces to Wetting by Water. *Ind. Eng. Chem.* **1936**, *28*, 988–994.
- Jung, Y. C.; Bhushan, B. Dynamic Effects of Bouncing Water Droplets on Superhydrophobic Surfaces. *Langmuir* **2008**, *24*, 6262–6269.
- Maitra, T.; Tiwari, M. K.; Antonini, C.; Schoch, P.; Jung, S.; Eberle, P.; Poulikakos, D. On the Nanoengineering of Superhydrophobic and Impalement Resistant Surface Textures below the Freezing Temperature. *Nano Lett.* **2014**, *14*, 172–182.
- Richard, D.; Clanet, C.; Quéré, D. Surface Phenomena Contact Time of a Bouncing Drop. *Nature* **2002**, *417*, 811–812.
- Clanet, C.; Béguin, C.; Richard, D.; Quéré, D. Maximal Deformation of an Impacting Drop. *J. Fluid Mech.* **2004**, *517*, 199–208.
- Bird, J. C.; Dhiman, R.; Kwon, H.-M.; Varanasi, K. K. Reducing the Contact Time of a Bouncing Drop. *Nature* **2013**, *503*, 385–388.
- Wang, H. J.; Xi, X. K.; Kleinhammes, A.; Wu, Y. Temperature-Induced Hydrophobic–Hydrophilic Transition Observed by Water Adsorption. *Science* **2008**, *322*, 80–83.
- Hummer, G.; Rasaiah, J. C.; Noworyta, J. P. Water Conduction through the Hydrophobic Channel of a Carbon Nanotube. *Nature* **2001**, *414*, 188–190.

61. Wang, C.; Lu, H.; Wang, Z.; Xiu, P.; Zhou, B.; Zuo, G.; Wan, R.; Hu, J.; Fang, H. Stable Liquid Water Droplet on a Water Monolayer Formed at Room Temperature on Ionic Model Substrates. *Phys. Rev. Lett.* **2009**, *103*, 137801.

62. Wang, C.; Zhou, B.; Tu, Y.; Duan, M.; Xiu, P.; Li, J.; Fang, H. Critical Dipole Length for the Wetting Transition Due to Collective Water-Dipoles Interactions. *Sci. Rep.* **2012**, *2*, 358.

63. Viovy, J.; Beynsens, D.; Knobler, C. Scaling Description for the Growth of Condensation Patterns on Surfaces. *Phys. Rev. A* **1988**, *37*, 4965–4970.

64. Narhe, R.; Beynsens, D. Nucleation and Growth on a Superhydrophobic Grooved Surface. *Phys. Rev. Lett.* **2004**, *93*, 076103.

65. Quéré, D.; Lafuma, A.; Quéré, D. Superhydrophobic States. *Nat. Mater.* **2003**, *2*, 457–460.

66. He, M.; Li, H.; Wang, J.; Song, Y. Superhydrophobic Surface at Low Surface Temperature. *Appl. Phys. Lett.* **2011**, *98*, 093118.

67. Söhnle, O.; Mullin, J. W. Interpretation of Crystallization Induction Periods. *J. Colloid Interface Sci.* **1988**, *123*, 43–50.

68. Franks, F.; Darlington, J.; Schenz, T.; Mathias, S.; Slade, L.; Levine, H. Antifreeze Activity of Antarctic Fish Glycoprotein and a Synthetic Polymer. *Nature* **1987**, *325*, 146–147.

69. Suzuki, S.; Nakajima, A.; Yoshida, N.; Sakai, M.; Hashimoto, A.; Kameshima, Y.; Okada, K. Freezing of Water Droplets on Silicon Surfaces Coated with Various Silanes. *Chem. Phys. Lett.* **2007**, *445*, 37–41.

70. Alizadeh, A.; Yamada, M.; Li, R.; Shang, W.; Otta, S.; Zhong, S.; Ge, L.; Dhinojwala, A.; Conway, K. R.; Bahadur, V.; et al. Dynamics of Ice Nucleation on Water Repellent Surfaces. *Langmuir* **2012**, *28*, 3180–3186.

71. Jung, S.; Tiwari, M. K.; Doan, N. V.; Poulikakos, D. Mechanism of Supercooled Droplet Freezing on Surfaces. *Nat. Commun.* **2012**, *3*, 615.

72. Li, K.; Xu, S.; Shi, W.; He, M.; Li, H.; Li, S.; Zhou, X.; Wang, J.; Song, Y. Investigating the Effects of Solid Surfaces on Ice Nucleation. *Langmuir* **2012**, *28*, 10749–10754.

73. Webster, J.; Davey, R. A.; Duller, G. A.; Ingold, C. T. Ballistospore Discharge in *Itersonilia perplexans*. *Trans. Br. Mycol. Soc.* **1984**, *82*, 13–29.

74. Pringle, A.; Patek, S. N.; Fischer, M.; Stolze, J.; Money, N. P. The Captured Launch of a Ballistospore. *Mycologia* **2005**, *94*, 866–871.

75. Boreyko, J.; Chen, C. H. Self-Propelled Dropwise Condensate on Superhydrophobic Surfaces. *Phys. Rev. Lett.* **2009**, *103*, 184501.

76. He, M.; Zhou, X.; Zeng, X.; Cui, D.; Zhang, Q.; Chen, J.; Li, H.; Wang, J.; Cao, Z.; Song, Y.; et al. Hierarchically Structured Porous Aluminum Surfaces for High-Efficient Removal of Condensed Water. *Soft Matter* **2012**, *8*, 6680–6683.

77. McKinley, G. H.; Renardy, M. Wolfgang Von Ohnesorge. *Phys. Fluids* **2011**, *23*, 127101.

78. Miljkovic, N.; Preston, D. J.; Enright, R.; Wang, E. N. Electrostatic Charging of Jumping Droplets. *Nat. Commun.* **2013**, *4*, 2517.

79. Boreyko, J. B.; Collier, C. P. Delayed Frost Growth on Jumping-Drop Superhydrophobic Surfaces. *ACS Nano* **2013**, *7*, 1618–1627.

80. Wier, K. A.; McCarthy, T. J. Condensation on Ultrahydrophobic Surfaces and Its Effect on Droplet Mobility: Ultrahydrophobic Surfaces Are Not Always Water Repellant. *Langmuir* **2006**, *22*, 2433–2436.

81. Miljkovic, N.; Enright, R.; Nam, Y.; Lopez, K.; Dou, N.; Sack, J.; Wang, E. N. Jumping-Droplet-Enhanced Condensation on Scalable Superhydrophobic Nanostructured Surfaces. *Nano Lett.* **2013**, *13*, 179–187.

82. Zhang, Q.; He, M.; Chen, J.; Wang, J.; Song, Y.; Jiang, L. Anti-Icing Surfaces Based on Enhanced Self-Propelled Jumping of Condensed Water Microdroplets. *Chem. Commun.* **2013**, *49*, 4516–4518.

83. Guadarrama-Cetina, J.; Mongruel, A.; González-Viñas, W.; Beynsens, D. Percolation-Induced Frost Formation. *Europhys. Lett.* **2013**, *101*, 16009.

84. Chen, X.; Ma, R.; Zhou, H.; Zhou, X.; Che, L.; Yao, S.; Wang, Z. Activating the Microscale Edge Effect in a Hierarchical Surface for Frosting Suppression and Defrosting Promotion. *Sci. Rep.* **2013**, *3*, 2515.

85. Zhang, Q.; He, M.; Zeng, X.; Li, K.; Cui, D.; Chen, J.; Wang, J.; Song, Y.; Jiang, L. Condensation Mode Determines the Freezing of Condensed Water on Solid Surfaces. *Soft Matter* **2012**, *8*, 8285–8288.

86. Zheng, L.; Li, Z.; Bourdo, S.; Khedir, K. R.; Asar, M. P.; Ryerson, C. C.; Biris, A. S. Exceptional Superhydrophobicity and Low Velocity Impact Icophobicity of Acetone-Functionalized Carbon Nanotube Films. *Langmuir* **2011**, *27*, 9936–9943.

87. Guo, P.; Zheng, Y.; Wen, M.; Song, C.; Lin, Y.; Jiang, L. Icophobic/Anti-Icing Properties of Micro/Nanostructured Surfaces. *Adv. Mater.* **2012**, *24*, 2642–2648.

88. Ruan, M.; Li, W.; Wang, B.; Deng, B.; Ma, F.; Yu, Z. Preparation and Anti-icing Behavior of Superhydrophobic Surfaces on Aluminum Alloy Substrates. *Langmuir* **2013**, *29*, 8482–8491.

89. Dotan, A.; Dodiuk, H.; Laforte, C.; Kenig, S. The Relationship between Water Wetting and Ice Adhesion. *J. Adhes. Sci. Technol.* **2009**, *23*, 1907–1915.

90. Wang, Y.; Xue, J.; Wang, Q.; Chen, Q.; Ding, J. Verification of Icophobic/Anti-icing Properties of a Superhydrophobic Surface. *ACS Appl. Mater. Interfaces* **2013**, *5*, 3370–3381.

91. Boreyko, J. B.; Srijanto, B. R.; Nguyen, T. D.; Vega, C.; Fuentes-Cabrera, M.; Collier, C. P. Dynamic Defrosting on Nanostructured Superhydrophobic Surfaces. *Langmuir* **2013**, *29*, 9516–9524.

92. Kulinich, S. A.; Farhadi, S.; Nose, K.; Du, X. W. Superhydrophobic Surfaces: Are They Really Ice-Repellent. *Langmuir* **2011**, *27*, 25–29.

93. Farhadi, S.; Farzaneh, M.; Kulinich, S. A. Anti-Icing Performance of Superhydrophobic Surfaces. *Appl. Surf. Sci.* **2011**, *257*, 6264–6269.

94. Varanasi, K. K.; Deng, T.; Smith, J. D.; Hsu, M.; Bhate, N. Frost Formation and Ice Adhesion on Superhydrophobic Surfaces. *Appl. Phys. Lett.* **2010**, *97*, 234102.

95. Stone, H. A. Ice-Phobic Surfaces That Are Wet. *ACS Nano* **2012**, *6*, 6536–6540.

96. Chen, J.; Liu, J.; He, M.; Li, K.; Cui, D.; Zhang, Q.; Zeng, X.; Zhang, Y.; Wang, J.; Song, Y. Superhydrophobic Surfaces Cannot Reduce Ice Adhesion. *Appl. Phys. Lett.* **2012**, *101*, 111603.

97. Jellinek, H. H. G. Adhesive Properties of Ice. *Journal of colloid science* **1959**, *14*, 268–280.

98. Nosonovsky, M.; Hejazi, V.; Sobolev, K.; Nosonovsky, M. From Superhydrophobicity to Icophobicity: Forces and Interaction Analysis. *Sci. Rep.* **2013**, *3*, 2194.

99. Nosonovsky, M.; Hejazi, V. Why Superhydrophobic Surfaces Are Not Always Icophobic. *ACS Nano* **2012**, *6*, 8488–8491.

100. Sarkar, D. K.; Farzaneh, M. Superhydrophobic Coatings with Reduced Ice Adhesion. *J. Adhes. Sci. Technol.* **2009**, *23*, 1215–1237.

101. Wang, F.; Lv, F.; Liu, Y.; Li, C.; Lv, Y. Ice Adhesion on Different Microstructure Superhydrophobic Aluminum Surfaces. *J. Adhes. Sci. Technol.* **2013**, *27*, 58–67.

102. Laforte, C.; Beisswenger, A. Icophobic Material Centrifuge Adhesion Test. *Proceedings of the 11th International Workshop on Atmospheric Icing of Structures*, Montréal, Canada, 2005; 1–6.

103. Kulinich, S. A.; Farzaneh, M. Ice Adhesion on Superhydrophobic Surfaces. *Appl. Surf. Sci.* **2009**, *255*, 8153–8157.

104. Kulinich, S. A.; Farzaneh, M. On Ice-Releasing Properties of Rough Hydrophobic Coatings. *Cold Reg. Sci. Technol.* **2011**, *65*, 60–64.

105. Chen, J.; Dou, R.; Cui, D.; Zhang, Q.; Zhang, Y.; Xu, F.; Zhou, X.; Wang, J.; Song, Y.; Jiang, L. Robust Prototypical Anti-Icing Coatings with a Self-Lubricating Liquid Water Layer between Ice and Substrate. *ACS Appl. Mater. Interfaces* **2013**, *5*, 4026–4030.

106. Susoff, M.; Siegmann, K.; Pfaffenroth, C.; Hirayama, M. Evaluation of Icophobic Coatings-Screening of Different Coatings and Influence of Roughness. *Appl. Surf. Sci.* **2013**, *282*, 870–879.

107. Wong, T. S.; Kang, S. H.; Tang, S. K. Y.; Smythe, E. J.; Hatton, B. D.; Grinthal, A.; Aizenberg, J. Bioinspired Self-Repairing Slippery Surfaces with Pressure-Stable Omniphobicity. *Nature* **2011**, *477*, 443–447.

108. Bohn, H. F.; Federle, W. Insect Aquaplaning: Nepenthes Pitcher Plants Capture Prey with The Peristome, a Fully Wettable Water-Lubricated Anisotropic Surface. *Proc. Natl. Acad. Sci. U. S. A.* **2004**, *101*, 14138–14143.

109. Varanasi, K. K.; Rykaczewski, K.; Anand, S.; Subramanyam, S. B.; Varanasi, K. K. Mechanism of Frost Formation on Lubricant-Impregnated Surfaces. *Langmuir* **2013**, *29*, 5230–5238.

110. Kim, P.; Wong, T. S.; Alvarenga, J.; Kreder, M. J.; Adorno-Martinez, W. E.; Aizenberg, J. Liquid-Infused Nanostructured Surfaces with Extreme Anti-Ice and Anti-Frost Performance. *ACS Nano* **2012**, *6*, 6569–6577.

111. Wilson, P. W.; Lu, W.; Xu, H.; Kim, P.; Kreder, M. J.; Alvarenga, J.; Aizenberg, J. Inhibition of Ice Nucleation by Slippery Liquid-Infused Porous Surfaces (SLIPS). *Phys. Chem. Chem. Phys.* **2013**, *15*, 581–585.

112. Nosonovsky, M. Materials Science: Slippery When Wetted. *Nature* **2011**, *477*, 412–413.

113. Smith, J. D.; Dhiman, R.; Anand, S.; Reza-Garduno, E.; Cohen, R. E.; McKinley, G. H.; Varanasi, K. K. Droplet Mobility on Lubricant-Impregnated Surfaces. *Soft Matter* **2013**, *9*, 1772–1780.

114. Subramanyam, S. B.; Rykaczewski, K.; Varanasi, K. K. Ice Adhesion on Lubricant-Impregnated Textured Surfaces. *Langmuir* **2013**, *29*, 13414–13418.

115. Anand, S.; Paxson, A. T.; Dhiman, R.; Smith, J. D.; Varanasi, K. K. Enhanced Condensation on Lubricant-Impregnated Nanotextured Surfaces. *ACS Nano* **2012**, *6*, 10122–10129.

116. Vogel, N.; Belisle, R. A.; Hatton, B.; Wong, T.-S.; Aizenberg, J. Transparency and Damage Tolerance of Patternable Omniphobic Lubricated Surfaces Based on Inverse Colloidal Monolayers. *Nat. Commun.* **2013**, *4*, 2176.

117. Ikeda-Fukazawa, T.; Kawamura, K. Molecular-Dynamics Studies of Surface of Ice Ih. *J. Chem. Phys.* **2004**, *120*, 1395–1401.

118. Kietzig, A. M.; Hatzikirakos, S. G.; Englezos, P. Physics of Ice Friction. *J. Appl. Phys.* **2010**, *107*, 081101.

119. Rosenberg, R. Why Is Ice Slippery? *Phys. Today* **2005**, *58*, 50.

120. Koop, T.; Luo, B.; Tsias, A.; Peter, T. Water Activity as The Determinant for Homogeneous Ice Nucleation in Aqueous Solutions. *Nature* **2000**, *406*, 611–614.

121. DeVries, A. L.; Wohlschlag, D. E. Freezing Resistance in Some Antarctic Fishes. *Science* **1969**, *163*, 1073–1075.

122. Graether, S. P.; Kuiper, M. J.; Gagné, S. M.; Walker, V. K.; Jia, Z.; Sykes, B. D.; Davies, P. L.  $\beta$ -Helix Structure and Ice-Binding Properties of a Hyperactive Antifreeze Protein from an Insect. *Nature* **2000**, *406*, 325–328.

123. Duman, J. G. The Role of Macromolecular Antifreeze in the Darkling Beetle *Meracantha contracta*. *J. Comp. Physiol.* **1977**, *115*, 279–286.

124. Duman, J. G.; Olsen, T. M. Thermal Hysteresis Protein Activity in Bacteria, Fungi, and Phylogenetically Diverse Plants. *Cryobiology* **1993**, *30*, 322–328.

125. Gilbert, J. A.; Hill, P. J.; Dodd, C. E.; Laybourn-Parry, J. Demonstration of Antifreeze Protein Activity in Antarctic Lake Bacteria. *Microbiology* **2004**, *150*, 171–180.

126. Urrutia, M. E.; Duman, J. G.; Knight, C. A. Plant Thermal Hysteresis Proteins. *Biochim. Biophys. Acta, Protein Struct. Mol. Enzymol.* **1992**, *1121*, 199–206.

127. Sidebottom, C.; Buckley, S.; Pudney, P.; Twigg, S.; Jarman, C.; Holt, C.; Telford, J.; McArthur, A.; Worrall, D.; Hubbard, R. Phytochemistry: Heat-Stable Antifreeze Protein from Grass. *Nature* **2000**, *406*, 256–256.

128. Krog, J. O.; Zachariassen, K. E.; Larsen, B.; Smidsrød, O. Thermal Buffering in Afro-Alpine Plants Due to Nucleating Agent-Induced Water Freezing. *Nature* **1979**, *282*, 300–301.

129. Zachariassen, K. E.; Kristiansen, E. Ice Nucleation and Antinucleation in Nature. *Cryobiology* **2000**, *41*, 257–279.

130. Kenisarin, M.; Mahkamov, K. Solar Energy Storage Using Phase Change Materials. *Renewable Sustainable Energy Rev.* **2007**, *11*, 1913–1965.

131. Bhamidipati, M. V. Methods and Compositions for Inhibiting Surface Icing. US 7514017, Apr. 7, 2009.

132. Duman, J. G. Antifreeze and Ice Nucleator Proteins in Terrestrial Arthropods. *Annu. Rev. Physiol.* **2001**, *63*, 327–357.

133. Meister, K.; Ebbinghaus, S.; Xu, Y.; Duman, J. G.; DeVries, A.; Gruebele, M.; Leitner, D. M.; Havenith, M. Long-Range Protein–Water Dynamics in Hyperactive Insect Antifreeze Proteins. *Proc. Natl. Acad. Sci. U. S. A.* **2013**, *110*, 1617–1622.

134. Raymond, J. A.; DeVries, A. L. Adsorption Inhibition as a Mechanism of Freezing Resistance in Polar Fishes. *Proc. Natl. Acad. Sci. U. S. A.* **1977**, *74*, 2589–2593.

135. Yeh, Y.; Feeney, R. E. Antifreeze Proteins: Structures and Mechanisms of Function. *Chem. Rev.* **1996**, *96*, 601–618.

136. Nutt, D. R.; Smith, J. C. Dual Function of the Hydration Layer around an Antifreeze Protein Revealed by Atomistic Molecular Dynamics Simulations. *J. Am. Chem. Soc.* **2008**, *130*, 13066–13073.

137. Meister, K.; Ebbinghaus, S.; Xu, Y.; Duman, J. G.; DeVries, A.; Gruebele, M.; Leitner, D. M.; Havenith, M. Long-Range Protein–Water Dynamics in Hyperactive Insect Antifreeze Proteins. *Proc. Natl. Acad. Sci. U. S. A.* **2013**, *110*, 1617–1622.

138. Meldolesi, A. GM Fish Ice Cream. *Nat. Biotechnol.* **2009**, *27*, 682–682.

139. Esser-Kahn, A. P.; Trang, V.; Francis, M. B. Incorporation of Antifreeze Proteins into Polymer Coatings Using Site-Selective Bioconjugation. *J. Am. Chem. Soc.* **2010**, *132*, 13264–13269.

140. Peltier, R.; Brimble, M. A.; Wojnar, J. M.; Williams, D. E.; Evans, C. W.; DeVries, A. L. Synthesis and Antifreeze Activity of Fish Antifreeze Glycoproteins and Their Analogs. *Chem. Sci.* **2010**, *1*, 538–551.

141. Congdon, T.; Notman, R.; Gibson, M. I. Antifreeze (Glyco) protein Mimetic Behavior of Poly(vinyl alcohol): Detailed Structure Ice Recrystallization Inhibition Activity Study. *Biomacromolecules* **2013**, *14*, 1578–1586.

142. Dorrer, C.; Rühe, J. Some Thoughts on Superhydrophobic Wetting. *Soft Matter* **2009**, *5*, 51–61.

143. Yang, C.; Tartaglino, U.; Persson, B. Influence of Surface Roughness on Superhydrophobicity. *Phys. Rev. Lett.* **2006**, *97*, 116103.

144. Li, G. A. Liquid Metals: Supercool Order. *Nat. Mater.* **2006**, *5*, 13–14.

145. Schülli, T.; Daudin, R.; Renaud, G.; Vaysset, A.; Geaymond, O.; Pasturel, A. Substrate-Enhanced Supercooling in AuSi Eutectic Droplets. *Nature* **2010**, *464*, 1174–1177.

146. Antonini, C.; Bernagozzi, I.; Jung, S.; Poulikakos, D.; Marengo, M. Water Drops Dancing on Ice: How Sublimation Leads to Drop Rebound. *Phys. Rev. Lett.* **2013**, *111*, 014501.

147. Sun, T.; Qing, G. Biomimetic Smart Interface Materials for Biological Applications. *Adv. Mater.* **2011**, *23*, H57–H77.

148. Fu, Q.; Rama Rao, G.; Basame, S. B.; Keller, D. J.; Artyushkova, K.; Fulghum, J. E.; López, G. P. Reversible Control of Free Energy and Topography of Nanostructured Surfaces. *J. Am. Chem. Soc.* **2004**, *126*, 8904–8905.

149. Boreyko, J.; Chen, C. H. Restoring Superhydrophobicity of Lotus Leaves with Vibration-Induced Dewetting. *Phys. Rev. Lett.* **2009**, *103*, 174502.

150. Guo, Z.; Zhou, F.; Hao, J.; Liu, W. Stable Biomimetic Superhydrophobic Engineering Materials. *J. Am. Chem. Soc.* **2005**, *127*, 15670–15671.

151. Wu, Y.; Bekke, M.; Inoue, Y.; Sugimura, H.; Kitaguchi, H.; Liu, C.; Takai, O. Mechanical Drability of Ultra-Water-Repellent Thin Film by Microwave Plasma-Enhanced CVD. *Thin Solid Films* **2004**, *457*, 122–127.

152. Jiang, C.; Wang, X.; Gunawidjaja, R.; Lin, Y. H.; Gupta, M. K.; Kaplan, D. L.; Naik, R. R.; Tsukruk, V. V. Mechanical Properties of Robust Ultrathin Silk Fibroin Films. *Adv. Funct. Mater.* **2007**, *17*, 2229–2237.
153. Xiu, Y.; Liu, Y.; Hess, D. W.; Wong, C. Mechanically Robust Superhydrophobicity on Hierarchically Structured Si Surfaces. *Nanotechnology* **2010**, *21*, 155705.
154. Deng, X.; Mammen, L.; Zhao, Y.; Lellig, P.; Müllen, K.; Li, C.; Butt, H. J.; Vollmer, D. Transparent, Thermally Stable and Mechanically Robust Superhydrophobic Surfaces Made From Porous Silica Capsules. *Adv. Mater.* **2011**, *23*, 2962–2965.
155. Verho, T.; Bower, C.; Andrew, P.; Franssila, S.; Ikkala, O.; Ras, R. H. Mechanically Durable Superhydrophobic Surfaces. *Adv. Mater.* **2011**, *23*, 673–678.
156. Zhu, X.; Zhang, Z.; Men, X.; Yang, J.; Wang, K.; Xu, X.; Zhou, X.; Xue, Q. Robust Superhydrophobic Surfaces with Mechanical Durability and Easy Repairability. *J. Mater. Chem.* **2011**, *21*, 15793–15797.
157. Dash, S.; Alt, M. T.; Garimella, S. V. Hybrid Surface Design for Robust Superhydrophobicity. *Langmuir* **2012**, *28*, 9606–9615.
158. Guo, Z.; Liu, W.; Su, B.-L. Superhydrophobic Surfaces: From Natural to Biomimetic to Functional. *J. Colloid Interface Sci.* **2011**, *353*, 335–355.
159. Shirtcliffe, N. J.; McHale, G.; I Newton, M. The Superhydrophobicity of Polymer Surfaces: Recent Developments. *J. Polym. Sci., Part B: Polym. Phys.* **2011**, *49*, 1203–1217.
160. Azimi, G.; Dhiman, R.; Kwon, H.-M.; Paxson, A. T.; Varanasi, K. K. Hydrophobicity of Rare-Earth Oxide Ceramics. *Nat. Mater.* **2013**, *12*, 315–320.
161. Liu, M.; Wang, S.; Jiang, L. Bioinspired Multiscale Surfaces with Special Wettability. *MRS Bull.* **2013**, *38*, 375–382.